

# Structure from noise: Mental errors yield abstract representations of events

Christopher W. Lynn<sup>1</sup>, Ari E. Kahn<sup>2,3</sup>, & Danielle S. Bassett<sup>1,3,4,5,6,\*</sup>

<sup>1</sup>*Department of Physics & Astronomy, College of Arts & Sciences, University of Pennsylvania, Philadelphia, PA 19104, USA*

<sup>2</sup>*Department of Neuroscience, Perelman School of Medicine, University of Pennsylvania, Philadelphia, PA 19104, USA*

<sup>3</sup>*Department of Bioengineering, School of Engineering & Applied Science, University of Pennsylvania, Philadelphia, PA 19104, USA*

<sup>4</sup>*Department of Electrical & Systems Engineering, School of Engineering & Applied Science, University of Pennsylvania, Philadelphia, PA 19104, USA*

<sup>5</sup>*Department of Neurology, Perelman School of Medicine, University of Pennsylvania, Philadelphia, PA 19104, USA*

<sup>6</sup>*Department of Psychiatry, Perelman School of Medicine, University of Pennsylvania, Philadelphia, PA 19104, USA*

Humans are adept at uncovering abstract associations in the world around them, yet the underlying mechanisms remain poorly understood. Intuitively, learning the higher-order structure of statistical relationships should involve complex mental processes. Here we propose an alternative perspective: that higher-order associations instead arise from natural errors in learning and memory. Combining ideas from information theory and reinforcement learning, we derive a maximum entropy (or minimum complexity) model of people's internal representations of the transitions between stimuli. Importantly, our model (i) affords a concise analytic form, (ii) qualitatively explains the effects of transition network structure on human expectations, and (iii) quantitatively predicts human reaction times in probabilistic sequential motor tasks. Together, these results suggest that mental errors influence our abstract representations of the world in significant and predictable ways, with direct implications for the study and design of optimally learnable information sources.

## Introduction

Our experience of the world is punctuated in time by discrete events, all connected by an architecture of hidden forces and causes. In order to form expectations about the future, one of the brain's primary functions is to infer the statistical structure underlying past experiences.<sup>1-3</sup> In fact, even within the first year of life, infants reliably detect the frequency with which one phoneme follows another in spoken language.<sup>4</sup> By the time we reach adulthood, uncovering statistical relationships between items and events enables us to perform abstract reasoning,<sup>5</sup> identify visual patterns,<sup>6</sup> produce language,<sup>7</sup> develop social intuition,<sup>8,9</sup> and segment continuous streams of data into self-similar parcels.<sup>10</sup> Notably, each of these functions requires the brain to identify statistical regularities across a range of scales. It has long been known, for instance, that people are sensitive to differences in individual transition probabilities such as those between words or concepts; intuitively, people are surprised when they witness a rare transition.<sup>4,6</sup> Additionally, mounting evidence suggests that humans can also infer abstract (or higher-order) statistical structures, including hierarchical patterns within sequences of stimuli,<sup>11</sup> temporal regularities on both global and local scales,<sup>12,13</sup> abstract concepts within webs of semantic relationships,<sup>14</sup> and general features of sparse data.<sup>15</sup>

To study this wide range of statistical structures in a unified framework, scientists have increasingly employed the language of network science,<sup>16</sup> wherein stimuli or states are conceptualized as nodes in a graph with edges or connections representing possible transitions between them. In this way, a sequence of stimuli often reflects a random walk along an underlying transi-

tion network,<sup>17-19</sup> and we can begin to ask which network features give rise to variations in human learning and behavior. This perspective has been particularly useful, for example, in the study of artificial grammars,<sup>20</sup> wherein human subjects are tasked with inferring the grammar rules (i.e., the network of transitions between letters and words) underlying a fabricated language.<sup>21</sup> Complementary research in statistical learning has demonstrated that modules (i.e., communities of densely-connected nodes) within transition networks are reflected in brain imaging data<sup>22</sup> and give rise to stark shifts in human reaction times.<sup>23</sup> Together, these efforts have culminated in a general realization that people's internal representations of a transition structure are strongly influenced by its higher-order organization, even after controlling for variations in the first-order statistics.<sup>24,25</sup> But how does the brain learn these abstract network features? Does the inference of higher-order relationships require sophisticated hierarchical learning algorithms? Or instead, do natural errors in cognition yield a "blurry" representation, making the coarse-grained architecture readily apparent?

To answer these questions, here we propose a single driving hypothesis: that when building models of the world, the brain is finely-tuned to maximize accuracy while simultaneously minimizing computational complexity. Generally, this assumption stems from a rich history exploring the trade-off between brain function and computational cost,<sup>26,27</sup> from sparse coding principles at the neuronal level<sup>28</sup> to the competition between information integration and segregation at the whole-brain level<sup>29</sup> to the notion of exploration versus exploitation<sup>30</sup> and the speed-accuracy trade-off<sup>31</sup> at the behavioral level. To formalize our hypothesis, we employ the free energy principle,<sup>32</sup> which has become increasingly utilized to investigate functional constraints in the brain.<sup>33,34</sup> De-

spite this thorough treatment of the accuracy-complexity trade-off in neuroscience and psychology, the prevailing intuition in statistical learning maintains that the brain is either optimized to perform Bayesian inference,<sup>8,14,15</sup> which is inherently error free, or hierarchical learning,<sup>11,13,18,20</sup> which typically entails increased rather than decreased computational complexity. Here, we show that the competition between mental errors and computational complexity leads to a maximum entropy (or minimum complexity) model of people's internal representations of events.<sup>32,35</sup> As we decrease the complexity of our model, allowing mental errors to take effect, we find that higher-order features of the transition network organically come into focus while the fine-scale structure fades away, thus providing a concise mechanism explaining how people infer abstract statistical relationships. To a broad audience, our model provides an accessible mapping from statistical structures to human behaviors, with particular relevance for the study and design of optimally learnable transition networks – either between words in spoken and written language,<sup>20,21,35</sup> notes in music,<sup>36</sup> or even concepts in classroom lectures.<sup>37</sup>

### **Network effects on human expectations**

In the cognitive sciences, mounting evidence suggests that human expectations depend critically on the higher-order features of transition networks.<sup>17,18</sup> Here, we make this notion concrete with empirical evidence for higher-order network effects in a probabilistic sequential response task.<sup>24</sup> Specifically, we presented human subjects with sequences of stimuli on a computer screen, each stimulus depicting a row of five grey squares with one or two of the squares highlighted in red (Fig. 17a). In response to each stimulus, subjects were asked to press one or two computer keys

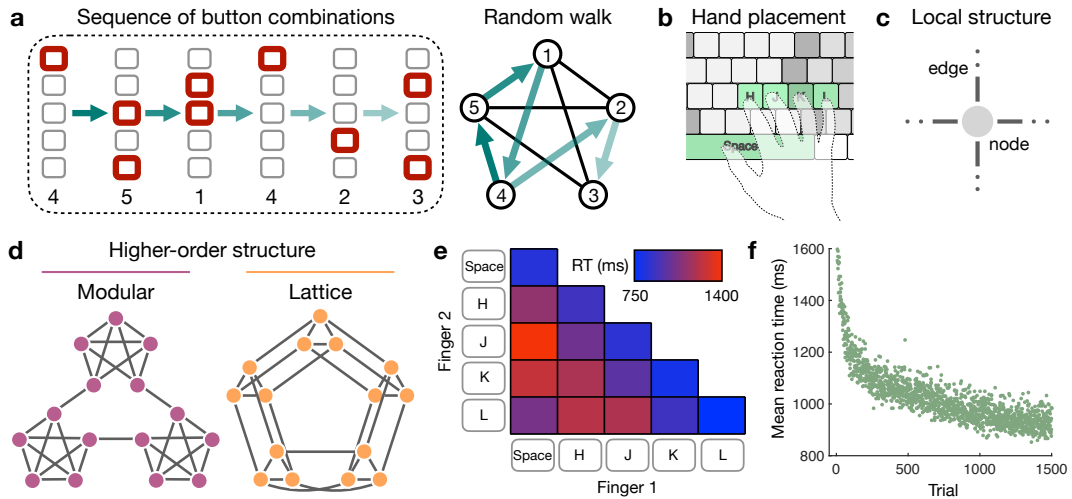


**Fig. 1: Subjects respond to sequences of stimuli drawn as a random walk on an underlying transition graph.**

**a**, Example sequence of visual stimuli (left) representing a random walk on an underlying transition network (right). **b**, For each stimulus, subjects are asked to respond by pressing a combination of one or two buttons on a keyboard. **c**, Each of the 15 possible button combinations corresponds to a node in the transition network. We only consider networks with nodes of uniform degree  $k = 4$  and edges with uniform transition probability 0.25. **d**, Subjects were asked to respond to sequences of 1500 such nodes drawn from two different transition architectures: a modular graph (left) and a lattice graph (right). **e**, Average reaction times across all subjects for the different button combinations, where the diagonal elements represent single-button presses and the off-diagonal elements represent two-button presses. **f**, Average reaction times as a function of trial number, characterized by a steep drop-off in the first 500 trials followed by a gradual decline in the remaining 1000 trials.

mirroring the highlighted squares (Fig. 17b). Each of the 15 different stimuli represented a node in an underlying transition network, upon which a random walk stipulated the sequential order of stimuli (Fig. 17a). Importantly, by measuring the speed with which a subject responded to each stimulus, we were able to infer their expectations about the transition structure – a fast reaction reflected a strongly-anticipated transition, while a slow reaction reflected a weakly-anticipated (or surprising) transition.<sup>1,2,24,38</sup>

While it has long been known that humans can detect differences in transition probabilities – for instance, rare transitions lead to sharp increases in reaction times<sup>4,6</sup> – more recently it has become clear that people’s expectations also reflect the higher-order architecture of transition networks.<sup>22–24,39</sup> To clearly study these higher-order effects without the complicating influence of edge weight variability, here we only consider transition graphs with a uniform transition probability of 0.25 on each edge, thereby requiring nodes to have uniform degree  $k = 4$  (Fig. 17c). Specifically, we consider two different graph topologies: a *modular* graph with three communities of five densely-connected nodes and a *lattice* graph representing a  $3 \times 5$  grid with periodic boundary conditions (Fig. 17d). Since both graphs have the same local structure (i.e., uniform node degree and edge weight), we stress that any systematic difference in reaction times between different parts of a graph, or between the two graphs themselves, must stem from expectations about their higher-order modular or lattice structure.

Regressing out the dependence of reaction times on the different button combinations (Fig. 17e) as well as the natural quickening of reactions with time<sup>40</sup> (Fig. 17f; see Methods), we identify two effects of higher-order network structure on subjects’ reactions. First, in the modular graph we find that reactions corresponding to within-cluster transitions are 50 ms faster than reactions to between-cluster transitions ( $p < 0.001$ ; Supplementary Tab. 1), an effect known as the *cross-cluster surprisal*<sup>24,39</sup> (Fig. 2a). Second, across all transitions within each network, we find that reactions in the modular graph are 31 ms faster than those in the lattice graph ( $p < 0.001$ ; Supplementary Tab. 2), a phenomenon that we coin the *modular-lattice* effect (Fig. 2b). To ensure that these results are not simply driven by recency effects, we performed a separate experiment with

short sequences of stimuli drawn according to Hamiltonian walks interspersed within the standard sequences of random walks.<sup>22</sup> We find that the cross-cluster surprisal arises even within these Hamiltonian walks, thereby confirming that higher-order network effects cannot be explained by recency alone (Supplementary Tabs. 3 and 4). In addition to these effects on reaction times, we also find that the probability of an erroneous response (i.e., a person responding with an incorrect key combination) increases for between-cluster transitions relative to within-cluster transitions (Supplementary Tab. 5). Together, these results indicate that people’s internal anticipations of events depend critically on the higher-order architecture of a transition network. But how do people infer abstract features like community structure from sequences of stimuli? In what follows, we leverage ideas from information theory and reinforcement learning to argue that one answer to this question lies in understanding the subtle role of mental errors.

### **Network effects reveal errors in graph learning**

Thus far, we have implicitly assumed, as is common, that humans maintain an internal representation  $\hat{A}$  of the transition structure, where  $\hat{A}_{ij}$  represents the expected probability of transitioning from node  $i$  to node  $j$ . Given a running tally  $n_{ij}$  of the number of times each transition has occurred, one might naïvely expect that the human brain is optimized to learn the true transition structure as accurately as possible.<sup>41,42</sup> This common hypothesis is represented by the maximum likelihood estimate,<sup>43</sup> taking the simple form

$$\hat{A}_{ij}^{\text{MLE}} = \frac{n_{ij}}{\sum_k n_{ik}}. \quad (1)$$



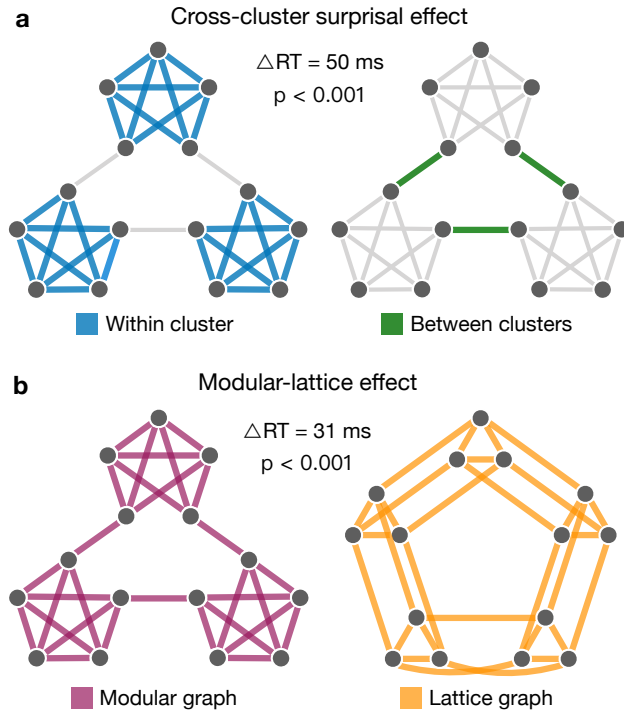


**Fig. 2: The effects of higher-order network structure on human reaction times.**

**a**, Cross-cluster surprisal effect in the modular graph, defined by an average increase in reaction times for between-cluster transitions (right) relative to within-cluster transitions (left). For results of statistical testing, see Supplementary Tab. 1. **b**, Modular-lattice effect, characterized by an overall increase in reaction times in the lattice graph (right) relative to the modular graph (left). For results of statistical testing, see Supplementary Tab. 2.

To see that human behavior does not reflect maximum likelihood estimation, we note simply that Eq. (1) provides an unbiased estimate of the transition structure;<sup>43</sup> that is, the estimated edge weights in  $\hat{A}^{\text{MLE}}$  are evenly distributed about their true value 0.25, independent of the higher-order transition structure. Thus, the fact that people's reaction times depend systematically on abstract features of the network marks a clear deviation from maximum likelihood estimation. To understand how higher-order network structure impacts people's internal representations, we must delve deeper into the learning process itself.

Consider a sequence of nodes  $(x_1, x_2, \dots)$ , where  $x_t \in \{1, \dots, N\}$  represents the node observed at time  $t$  and  $N$  is the size of the network (here  $N = 15$  for all graphs). To update the maximum likelihood estimate of the transition structure at time  $t + 1$ , one increments the counts  $n_{ij}$  using the following recursive rule,

$$n_{ij}(t + 1) = n_{ij}(t) + [i = x_t] [j = x_{t+1}], \quad (2)$$

where the Iverson bracket  $[\cdot] = 1$  if its argument is true and equals 0 otherwise. Importantly, we note that at each time  $t + 1$ , a person must recall the previous node that occurred at time  $t$ ; in other words, they must associate a cause  $x_t$  to each effect  $x_{t+1}$  that they observe. While maximum likelihood estimation requires perfect recollection of the previous node at each step, human errors in perception and recall are inevitable.<sup>44-46</sup> A more plausible scenario is that, when attempting to recall the node at time  $t$ , a person instead remembers the node at time  $t - \Delta t$  with some decreasing probability  $P(\Delta t)$ , where  $\Delta t \geq 0$ . This memory distribution, in turn, generates an internal belief about which node occurred at time  $t$ ,

$$B_t(i) = \sum_{\Delta t=0}^{t-1} P(\Delta t) [i = x_{t-\Delta t}]. \quad (3)$$

Updating Eq. (2) accordingly, we arrive at a new learning rule that accounts for natural errors in perception and recall,

$$\tilde{n}_{ij}(t + 1) = \tilde{n}_{ij}(t) + B_t(i) [j = x_{t+1}]. \quad (4)$$

Using this revised counting rule, we can begin to form more realistic predictions about people's internal estimates of the transition structure,  $\hat{A}_{ij} = \tilde{n}_{ij} / \sum_k \tilde{n}_{ik}$ .

We pause to emphasize that  $P(\Delta t)$  does not represent the forgetting of past stimuli alto-

gether; instead, it reflects the local shuffling of stimuli in time. In fact, if one were to simply forget past stimuli at some fixed rate – a process recently shown to play a vital role in other cognitive tasks<sup>47</sup> – this would merely introduce white noise into the maximum likelihood estimate  $\hat{A}^{\text{MLE}}$  (see Supplementary Information). By contrast, we will see that by shuffling the order of stimuli in time, people are able to gather information about the higher-order structure of the underlying transitions.

### **Choosing a memory distribution: The free energy principle**

In order to make predictions about people’s expectations, we must choose a particular mathematical form for the memory distribution  $P(\Delta t)$ . To do so, we begin with a single driving hypothesis: that the brain is finely-tuned to (i) minimize errors and (ii) minimize computational complexity. Formally, we define the error of a recalled stimulus to be its distance in time from the desired stimulus (i.e.,  $\Delta t$ ), such that the average error of a candidate distribution  $Q(\Delta t)$  is given by  $E(Q) = \sum_{\Delta t} Q(\Delta t)\Delta t$ . By contrast, it might seem difficult to formalize the computational complexity associated with storing and recalling events from a distribution  $Q$ . Intuitively, we would like the complexity of  $Q$  to increase with increasing certainty, and we would also like the complexity of two independent memory distributions to be additive. As famously shown by Shannon, these two criteria are sufficient to derive a quantitative definition of complexity<sup>35</sup> – namely, the negative entropy  $-S(Q) = \sum_{\Delta t} Q(\Delta t) \log Q(\Delta t)$ . All together, the total cost of a distribution  $Q$  is its free energy  $F(Q) = \beta E(Q) - S(Q)$ , where  $\beta$  is the inverse temperature parameter, which quantifies the relative value that the brain places on accuracy versus computational complexity.<sup>34</sup> In this way, our simple assumption about resource constraints in the brain necessarily leads to a particular form

for  $P$ : It must be the distribution that minimizes  $F(Q)$ , namely the Boltzmann distribution<sup>32</sup>

$$P(\Delta t) = \frac{1}{Z} e^{-\beta \Delta t}, \quad (5)$$

where  $Z$  is the normalizing constant or partition function (see Methods). Interestingly, free energy arguments similar to the one presented here have become increasingly utilized as a way to formalize constraints on cognitive functions,<sup>33,34</sup> with applications from bounded-rational decision making<sup>34</sup> to human action, perception, and learning under temporal or computational limitations.<sup>48–51</sup> Taken together, Eqs. (3-5) define our maximum entropy model of people’s internal transition estimates  $\hat{A}$ .

To gain an intuition for the model, we consider the infinite-time limit, such that the transition estimates become independent of the particular random walk chosen for analysis. Given a transition matrix  $A$ , one can show that the asymptotic estimates in our model are equivalent to an average over walks of various lengths,  $\hat{A} = \sum_{\Delta t} P(\Delta t) A^{\Delta t+1}$ , which, in turn, can be fashioned into the following analytic expression,

$$\hat{A} = (1 - e^{-\beta}) A (I - e^{-\beta} A)^{-1}, \quad (6)$$

where  $I$  is the identity matrix (see Methods). The model contains a single free parameter  $\beta$ , which represents the precision of a person’s mental representation. In the limit  $\beta \rightarrow \infty$  (no mental errors), our model becomes equivalent to maximum likelihood estimation (Fig. 3a), and the asymptotic estimates  $\hat{A}$  converge to the true transition structure  $A$  (Fig 3b), as expected.<sup>52</sup> Conversely, in the limit  $\beta \rightarrow 0$  (overwhelming mental errors), the memory distribution  $P(\Delta t)$  becomes uniform across all past nodes (Fig. 3a), and the mental representation  $\hat{A}$  loses all resemblance to the true structure  $A$

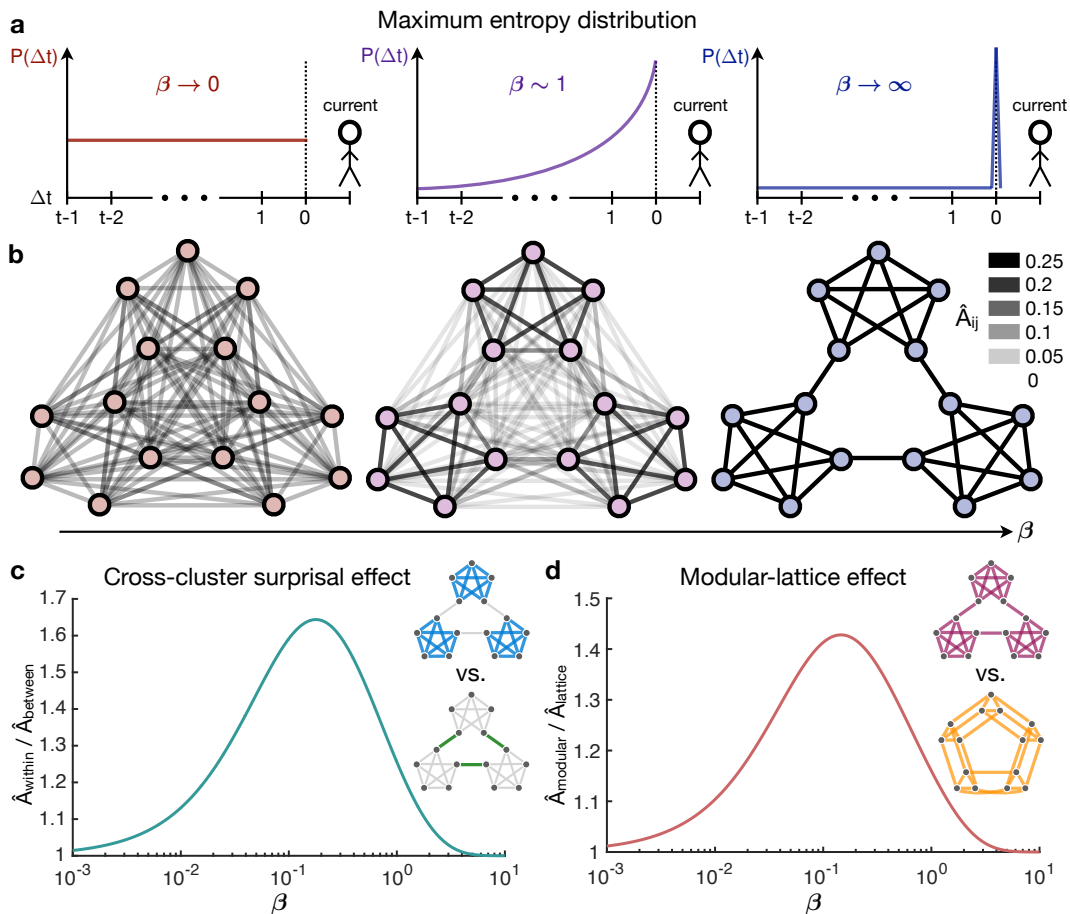


**Fig. 3: A maximum entropy model of transition probability estimates in humans.**

**a**, Illustration of the maximum entropy distribution  $P(\Delta t)$  representing the probability of recalling a stimulus  $\Delta t$  time steps from the target stimulus (dashed line). In the limit  $\beta \rightarrow 0$ , the distribution becomes uniform over all past stimuli (left). In the opposite limit  $\beta \rightarrow \infty$ , the distribution becomes a delta function on the desired stimuli (right). For intermediate amounts of noise, the distribution drops off monotonically (center). **b**, Resulting internal estimates  $\hat{A}$  of the transition structure. For  $\beta \rightarrow 0$ , the estimates become all-to-all, losing any resemblance to the true structure (left), while for  $\beta \rightarrow \infty$ , the transition estimates become exact (right). At intermediate precision, the higher-order community structure organically comes into focus (center). **c-d**, Predictions of the cross-cluster surprisal effect (panel **c**) and the modular-lattice effect (panel **d**) as functions of the inverse temperature  $\beta$ .

(Fig. 3b). Remarkably, however, for intermediate values of  $\beta$ , higher-order features of the transition network, such as communities of densely-connected nodes, come into sharper focus, while some of the fine-scale features, like the edges between communities, fade away (Fig. 3b). In fact, applying Eq. (6) to the modular graph, we find that the average expected probability of within-community transitions reaches over 1.6 times the estimated probability of between-community transitions (Fig. 3c), thus offering an explanation for the cross-cluster surprisal effect.<sup>24,39</sup> Furthermore, we find that the average estimated transition probabilities in the modular graph reach over 1.4 times the estimated probabilities in the lattice graph (Fig. 3d), thereby predicting the modular-lattice effect. In addition to these higher-order effects, we find that the model also explains previously reported variations in human expectations at the level of individual nodes<sup>4,6,24</sup> (Supplementary Fig. 1). Together, these results demonstrate that the maximum entropy model predicts the qualitative effects of network structure on human reaction times. But can we use the same ideas to quantitatively predict the behavior of particular individuals?

### **Predicting the behavior of individual humans**

In order to model the behavior of particular individuals, we must relate the transition estimates in Eqs. (3-5) to predictions about people's reaction times. Given a sequence of nodes  $x_1, \dots, x_{t-1}$ , we note that the reaction to the next node  $x_t$  is determined by the expected probability of transitioning from  $x_{t-1}$  to  $x_t$  calculated at time  $t - 1$ , which we denote by  $a(t) = \hat{A}_{x_{t-1}, x_t}(t - 1)$ . From this internal anticipation  $a(t)$ , the simplest possible prediction  $\hat{r}(t)$  for a person's reaction time is given by the linear relationship<sup>53</sup>  $\hat{r}(t) = r_0 + r_1 a(t)$ , where the intercept  $r_0$  represents a person's reaction

time with zero anticipation and the slope  $r_1$  quantifies the strength of the relationship between a person’s reactions and the internal representation in our model.<sup>54</sup> To estimate the parameters  $\beta$ ,  $r_0$ , and  $r_1$  that best describe a given individual, we minimize the RMS prediction error with respect to their observed reaction times after regressing out their button combination and trial number dependencies (Figs. 17e and 17f; see Methods). The distributions of the estimated parameters are shown in Fig. 4a. Among the 358 completed sequences in the modular and lattice graphs (across 214 subjects; see Methods), 44 were best described as performing maximum likelihood estimation ( $\beta \rightarrow \infty$ ) and 71 seemed to lack any notion of the transition structure whatsoever ( $\beta \rightarrow 0$ ), while among the remaining 243 sequences, the average inverse temperature was  $\beta = 0.31$ . Interestingly, this value of  $\beta$  roughly corresponds to that for which our model predicts the strongest network effects (Figs. 3c and 3d). In the following section, we will compare this value of  $\beta$  estimated indirectly from people’s reaction times with direct measurements of  $\beta$  in an independent experiment assessing human memory performance.

In addition to measuring  $\beta$ , we also wish to determine whether our model accurately describes individual behavior. Toward this end, we first note that the average slope  $r_1$  is large ( $r_1 = -1127$  ms), suggesting that the transition estimates in our model  $a(t)$  are strongly predictive of human reaction times, and negative, confirming the intuition that increased anticipation yields decreased reaction times (Fig. 4b). To quantitatively examine the accuracy of our framework, we compare our model against a hierarchy of competing models  $\hat{r}^{(\ell)}$ , which represent the hypothesis that humans learn explicit representations of the higher-order transition structure – an assumption that requires increased rather than decreased computational complexity relative to maximum like-

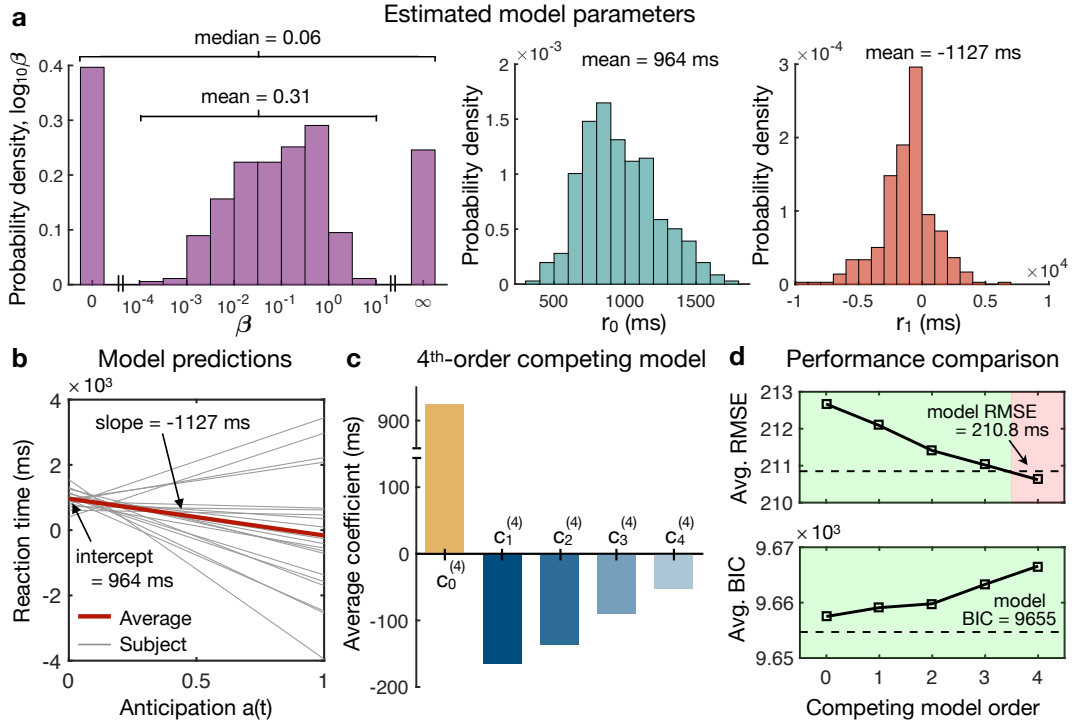


**Fig. 4: Predicting reaction times for individual subjects.**

**a**, Distributions of the estimated parameters for our maximum entropy model (i.e.,  $\hat{r}(t) = r_0 + r_1 a(t)$ ) across all 358 completed sequences. For the inverse temperature  $\beta$  (left), 44 subjects were best described as performing maximum likelihood estimation ( $\beta \rightarrow \infty$ ), 71 lacked any notion of the transition structure ( $\beta \rightarrow 0$ ), and the remaining 243 subjects had an average value of  $\beta = 0.31$ . The intercept  $r_0$  is positive, with an average value of 964 ms (center), while the slope  $r_1$  is strongly negative with an average value of  $-1127$  ms (right).

**b**, Predicted reaction time plotted as a function of a subject's internal anticipation. Grey lines indicate 20 randomly-selected subjects, and the red line shows the average prediction over all subjects.

**c**, Average linear parameters for the fourth-order competing model. Besides the intercept  $c_0^{(4)}$ , all coefficients are negative with increasingly higher-order transitions having progressively less predictive power.

**d**, Comparing the performance of our maximum entropy model with the hierarchy of competing models up to fourth-order. (Top) RMS error of our model averaged over subjects (dashed line) compared to the average RMS errors of the competing models (solid line); our model maintains higher accuracy than the competing hierarchy up to the third-order model. (Bottom) Average Bayesian information criterion (BIC) of the maximum entropy model (dashed line) compared to the average BIC of the competing models (solid line); our model provides the best description of the data across all models considered.



likelihood estimation. In particular, we denote the  $\ell^{\text{th}}$ -order transition matrix by  $\hat{A}_{ij}^{(\ell)} = n_{ij}^{(\ell)} / \sum_k n_{ik}^{(\ell)}$ , where  $n_{ij}^{(\ell)}$  counts the number of observed transitions from node  $i$  to node  $j$  in  $\ell$  steps. We then define a hierarchy of models that take into account increasingly higher-order transition structures, such that the  $\ell^{\text{th}}$ -order model contains perfect information about transitions up to length  $\ell$ :

$$\begin{aligned}\hat{r}^{(0)}(t) &= c_0^{(0)}, \\ \hat{r}^{(1)}(t) &= c_0^{(1)} + c_1^{(1)} a^{(1)}(t), \\ &\vdots \\ \hat{r}^{(\ell)}(t) &= c_0^{(\ell)} + \sum_{k=1}^{\ell} c_k^{(\ell)} a^{(k)}(t),\end{aligned}\tag{7}$$

where  $a^{(k)}(t) = \hat{A}_{x_{t-1}, x_t}^{(k)}(t-1)$ . Generally, each model  $\hat{r}^{(\ell)}$  contains  $\ell + 1$  parameters  $c_0^{(\ell)}, \dots, c_\ell^{(\ell)}$ , where  $c_k^{(\ell)}$  quantifies the predictive power of the  $k^{\text{th}}$ -order transition structure. Intuitively, for each model  $\hat{r}^{(\ell)}$ , we expect  $c_1^{(\ell)}, c_2^{(\ell)}, \dots$  to be negative, reflecting a decrease in reaction times due to increased anticipation, and decreasing in magnitude, reflecting the intuition that higher-order transition structures should be progressively less predictive of people's reaction times. Indeed, considering the fourth-order model  $\hat{r}^{(4)}$  as an example, we find that progressively higher-order transition structures play decreasingly significant roles in shaping human reactions (Fig. 4c). However, even the largest coefficient in the fourth-order model ( $c_1^{(4)} = -165$  ms) is nearly an order of magnitude smaller than the slope in our model ( $r_1 = -1127$  ms), indicating that the representation  $\hat{A}$  in our model is much more strongly predictive of people's reaction times than any of the explicit representations  $\hat{A}^{(1)}, \hat{A}^{(2)}, \dots$  in the competing models. In fact, our maximum entropy model achieves higher accuracy than the first three orders of the competing model hierarchy (Fig. 4d) – this is despite the fact that the third-order model even contains one more parameter. To account for the

increasing number of parameters in the competing model hierarchy, we additionally compare the average Bayesian information criterion (BIC) of our model with the average BIC of the competing models, finding that the maximum entropy model provides the best description of the data across all models considered. Taken together, these results indicate that the free energy hypothesis, and the resulting maximum entropy model, are consistently more effective at describing human reactions than the hypothesis that people learn explicit representations of the higher-order transition structure.

### **Directly probing the memory distribution**

Throughout our discussion, we have argued that errors in memory shape human representations in predictable ways, a perspective that has received increasing attention in recent years.<sup>47,55,56</sup> While we have seen that this framework explains specific aspects of human behavior, we also note that there exist alternative perspectives that could be used to generate similar predictions. For example, one could imagine a Bayesian learner who assumes that the structure of the sequence is non-Markovian and therefore “integrates” the transition structure over time, even without sustaining errors in memory or learning. We arrive at a complementary viewpoint by noting that Eq. (6) resembles the successor representation in reinforcement learning,<sup>57,58</sup> which assumes that, rather than shuffling the order of past stimuli, humans are instead planning their responses multiple steps in advance (see Supplementary Information for an extended discussion). In order to distinguish our framework from these alternatives, here we provide direct evidence for precisely the types of mental errors that our model predicts.

In the construction and testing of our model, we have developed a number of predictions concerning the shape of the memory distribution  $P(\Delta t)$ , which, to recall, represents the probability of remembering the stimulus at time  $t - \Delta t$  instead of the target stimulus at time  $t$ . We first assumed, as one would intuitively expect, that  $P(\Delta t)$  decreases monotonically in  $\Delta t$ . Second, in order to make quantitative predictions, we employed the free energy principle, leading to the specific prediction that  $P$  drops off exponentially quickly with  $\Delta t$  (Eq. (5)). Finally, when describing the reaction times of individual subjects, we estimated an average value for the inverse temperature  $\beta$  of 0.31. To test these three predictions directly, we conducted a standard  $n$ -back memory experiment. Specifically, we presented subjects with sequences of letters on a screen, and they were asked to respond to each letter indicating whether or not it was the same as the letter that occurred  $n$  steps previously; for each subject, this process was repeated for the three conditions  $n = 1, 2$ , and 3. To measure the memory distribution  $P(\Delta t)$ , we considered all trials on which a subject responded positively that the current stimulus matched the target. For each such trial, we looked back to the last time that the subject did in fact observe the current stimulus and we recorded the distance (in trials) between this observation and the target (Fig. 5a). In this way, we were able to treat each positive response as a sample of  $\Delta t$  from the memory distribution  $P(\Delta t)$ .

The measurements of  $P$  for the 1-, 2-, and 3-back tasks are shown in Figure 5b, and the combined measurement of  $P$  across all conditions is shown in Figure 5c. Notably, the distributions decrease monotonically and maintain consistent exponential forms, even out to  $\Delta t = 10$  trials from the target stimulus, thereby providing direct evidence for the Boltzmann distribution (Eq. (5)) and the free energy principle more generally. Moreover, fitting an exponential curve

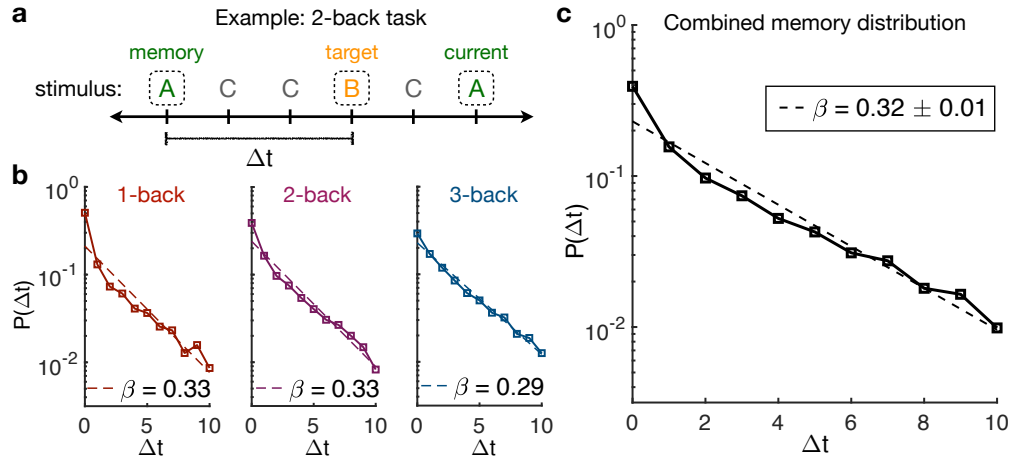


**Fig. 5: Measuring the memory distribution in an  $n$ -back experiment.**

**a**, Example of the 2-back memory task. Subjects view a sequence of stimuli (letters) and respond to each stimulus indicating whether it matches the target stimulus from two trials before. For each positive response that the current stimulus matches the target, we measure  $\Delta t$  by calculating the number of trials between the last instance of the current stimulus and the target. **b**, Histograms of  $\Delta t$  (i.e., measurements of the memory distribution  $P(\Delta t)$ ) across all subjects in the 1-, 2-, and 3-back tasks. Dashed lines indicate exponential fits to the observed distributions. The inverse temperature  $\beta$  is estimated for each task to be the negative slope of the exponential fit. **c**, Memory distribution aggregated across the three  $n$ -back tasks. Dashed line indicates an exponential fit. We report a combined estimate of the inverse temperature  $\beta = 0.32 \pm 0.01$ , where the standard deviation is estimated from 1,000 bootstrap samples of the combined data.

to each distribution, we can directly estimate the inverse temperature  $\beta$ . Remarkably, the value  $\beta = 0.32 \pm 0.1$  estimated from the combined distribution (Fig. 5c) matches (within errors) the average value  $\beta = 0.31$  estimated from people's reaction times in the serial response task (Fig. 4a). To further strengthen the link between mental errors and people's internal representations, we then asked the subjects to perform the original serial response task (Fig. 17), and for each subject, we estimated  $\beta$  using the two methods described above: First, we directly measured  $\beta$  by calculating an exponential fit to their individual memory distribution, and second, we indirectly estimated  $\beta$

based on their reactions in the serial response task. Comparing these two estimates across subjects, we find that they are significantly related with Spearman correlation  $r_s = 0.28$  ( $p = 0.047$ ; see Methods). When viewed in concert, these results demonstrate not only the existence of the particular form of mental errors predicted by our model – down to the specific value of  $\beta$  – but also the relationship between these mental errors and people’s internal estimates of the transition structure.

### **Learned network structure guides reactions to novel transitions**

Given a model that accurately describes human reactions to sequences of stimuli, it is ultimately interesting to make new predictions about human behavior. Thus far, in keeping with the majority of existing research,<sup>4,6,22–24,39</sup> we have focused exclusively on static transition graphs, wherein the probability  $A_{ij}$  of transitioning from state  $i$  to state  $j$  remains constant over time. However, the statistical structures governing human life are continually shifting,<sup>59,60</sup> and people are often forced to respond to rare or novel transitions.<sup>61,62</sup> Here we show that, when confronted with a novel transition – or a *violation* to the preexisting transition network – not only are people surprised, but the magnitude of their surprise depends critically on the topological length of the novel transition in the previously learned network. This result reveals that people implicitly learn the topological distances between all nodes in the transition graph, not just those pairs for which a transition has already been observed.

To easily interpret the effects of topological distance on human reactions, we consider a ring graph where each node is connected to its nearest and next-nearest neighbors (Fig. 6a). We asked

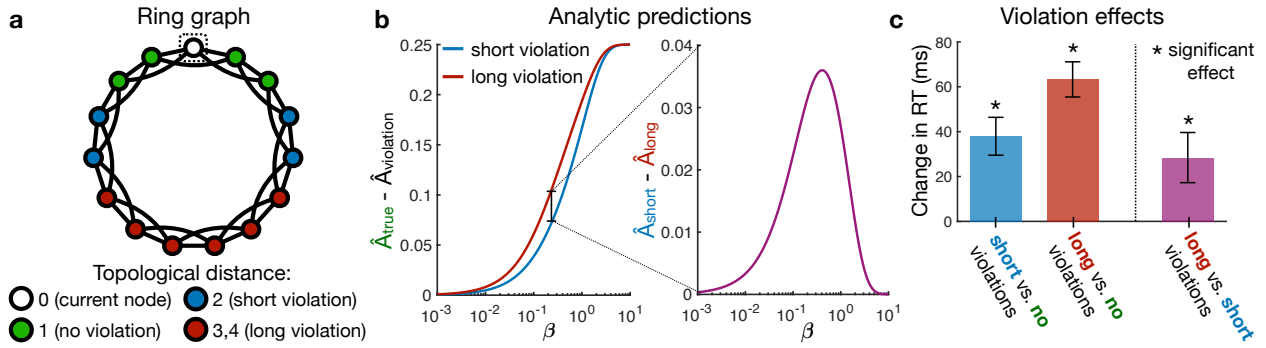


**Fig. 6: Network violations yield surprise that grows with topological distance.**

**a**, Ring graph consisting of 15 nodes, where each node is connected to its nearest neighbors and next-nearest neighbors on the ring. Starting from the boxed node, a sequence can undergo a standard transition (green), a short violation of the transition structure (blue), or a long violation (red). **b**, Our model predicts that subjects' anticipations of both short (blue) and long (red) violations should be weaker than their anticipations of standard transitions (left). Furthermore, we predict that subjects' anticipations of violations should decrease with increasing topological distance (right). **c**, Average effects of network violations across 78 subjects, estimated using a mixed effects model, with error bars indicating one standard deviation from the mean. We find that all network violations yield increased reaction times relative to standard transitions, with topologically distant violations inducing slower reactions than short violations, thus confirming the predictions of our model.

subjects to respond to sequences of 1500 nodes drawn as random walks on the ring graph, but with 50 violations randomly interspersed (see Methods). These violations were divided into two categories: short violations of topological distance two and long violations of topological distances three and four (Fig. 6a). Using maximum likelihood estimation (Eq. (1)) as a guide, one would naïvely expect people to be equally surprised by all violations – indeed, each violation has never been seen before. In contrast to this intuition, our model predicts that a person's surprise at the observation of a novel transition should depend crucially on that transition's topological distance in the underlying graph, with topologically longer violations inducing increased surprise over short

violations (Fig. 6b). In the data, we find that all violations give rise to sharp increases in reaction times relative to standard transitions (Fig. 6c; Supplementary Tab. 7), indicating that people are in fact learning the underlying transition structure. More importantly, we find that reaction times for long violations are 28 ms longer on average than those for short violations ( $p = 0.011$ ; Fig. 6c; Supplementary Tab. 8), even after accounting for recency effects (see Methods).<sup>63</sup> These results suggest that mental errors, while forcing human expectations to systematically deviate from reality, provide people with an implicit understanding of the topological scales in a transition network.<sup>59–62</sup>

## Conclusions and outlook

Daily life is filled with sequences of items that obey an underlying network architecture, from networks of word and note transitions in natural language and music to networks of abstract relationships in classroom lectures and literature.<sup>5–10</sup> How humans infer these complex structures from examples and how they represent the networks internally are questions of fundamental and general interest.<sup>11–15</sup> Recent experiments in statistical learning have established that human representations depend critically on the higher-order organization of probabilistic transitions, yet the underlying mechanisms remain poorly understood.<sup>22–25</sup> Here, we show that these network effects can be understood as stemming from mental errors in people’s estimates of the transition structure. Combining ideas from information theory and reinforcement learning, we propose a new model of human expectations based on the hypothesis that the brain is tuned to simultaneously minimize both errors and computational complexity.<sup>26–31,34,48–51</sup> This competition between accuracy and efficiency yields a noisy internal representation of the transitions between states, which, in turn,

explains with notable accuracy an array of higher-order network phenomena observed in human experiments.<sup>22–25</sup> Importantly, our model admits a concise analytic form that aids intuition (Eq. (6)) and, by estimating the inverse temperature  $\beta$  that best describes a particular individual, can be used to predict human behavior on a person-by-person basis.

Our work directly inspires new research directions, particularly with regard to the study and design of optimally learnable network structures. Given the notion that densely connected communities help to mitigate the effects of mental errors on people’s internal representations, we anticipate that networks with high “learnability” will possess a hierarchical community structure.<sup>64</sup> Interestingly, such hierarchical organization has already been observed in a diverse range of real world structures, from knowledge and language networks<sup>65</sup> to social networks and the World Wide Web.<sup>66</sup> Could it be that these networks have evolved so as to facilitate accurate representations in the minds of the humans observing and building them? Questions such as this demonstrate the importance of having simple predictive models of human representations and point to the promising future of this research endeavor.

## Methods

**Derivation of the maximum entropy model and the infinite-sequence limit.** Here we provide a more thorough derivation of our maximum entropy model of human expectations, with the goal of fostering intuition. Given a matrix of erroneous transition counts  $\tilde{n}_{ij}$ , our estimate of the transition structure is given by  $\hat{A}_{ij} = \tilde{n}_{ij} / \sum_k \tilde{n}_{ik}$ . When observing a sequence of nodes  $x_1, x_2, \dots$ , in order to construct the counts  $\tilde{n}_{ij}$ , we assume that humans use the following recursive rule:  $\tilde{n}_{ij}(t+1) = \tilde{n}_{ij}(t) + B_t(i)[j = x_{t+1}]$ , where  $B_t(i)$  denotes the belief, or perceived probability, that node  $i$  occurred at the previous time  $t$ . This belief, in turn, can be written in terms of the



probability  $P(\Delta t)$  of accidentally recalling the node that occurred  $\Delta t$  time steps from the desired node at time  $t$ :

$$B_t(i) = \sum_{\Delta t=0}^{t-1} P(\Delta t) [i = x_{t-\Delta t}].$$

In order to make quantitative predictions about people's estimates of a transition structure, we must choose a mathematical form for  $P(\Delta t)$ . To do so, we leverage the free energy principle<sup>34</sup>: When building mental models, the brain is finely-tuned to simultaneously minimize errors and computational complexity. The average error associated with a candidate distribution  $Q(\Delta t)$  is assumed to be the average distance in time of the recalled node from the target node, denoted  $E(Q) = \sum_{\Delta t} Q(\Delta t)\Delta t$ . Furthermore, Shannon famously proved that the only suitable choice for the computational cost of a candidate distribution is its negative entropy,<sup>35</sup> denoted  $-S(Q) = \sum_{\Delta t} Q(\Delta t) \log Q(\Delta t)$ . Taken together, the total cost associated with a distribution  $Q(\Delta t)$  is given by the free energy  $F(Q) = \beta E(Q) - S(Q)$ , where  $\beta$ , referred to as the inverse temperature, parameterizes the relative importance of minimizing errors versus computational costs. By minimizing  $F$  with respect to  $Q$ , we arrive at the Boltzmann distribution  $P(\Delta t) = e^{-\beta \Delta t} / Z$ , where  $Z$  is the normalizing partition function.<sup>32</sup> We emphasize that this mathematical form for  $P(\Delta t)$  followed necessarily from our free energy assumption about the functionality of the brain.

To gain an analytic intuition for the model without referring to a particular random walk, we consider the limit of an infinitely long sequence of nodes. To begin, we consider a sequence  $x_1, \dots, x_T$  of length  $T$ . At the end of this sequence, the counting matrix takes the form

$$\begin{aligned} \tilde{n}_{ij}(T) &= \sum_{t=1}^{T-1} B_t(i) [j = x_{t+1}] \\ &= \sum_{t=1}^{T-1} \left( \sum_{\Delta t=0}^{t-1} P(\Delta t) [i = x_{t-\Delta t}] \right) [j = x_{t+1}]. \end{aligned} \quad (8)$$

Dividing both sides by  $T$ , the right-hand side becomes a time average, which by the ergodic theorem converges to an expectation over the transition structure in the limit  $T \rightarrow \infty$ ,

$$\lim_{T \rightarrow \infty} \frac{\tilde{n}_{ij}(T)}{T} = \sum_{\Delta t=0}^{\infty} P(\Delta t) \langle [i = x_{t-\Delta t}] [j = x_{t+1}] \rangle_A, \quad (9)$$

where  $\langle \cdot \rangle_A$  denotes an expectation over random walks in  $A$ . We note that the expectation of an identity function is simply a probability, such that  $\langle [i = x_{t-\Delta t}] [j = x_{t+1}] \rangle_A = p_i (A^{\Delta t+1})_{ij}$ , where  $p_i$  is the long-run probability of node  $i$  appearing in the sequence and  $(A^{\Delta t+1})_{ij}$  is the probability of randomly walking from node  $i$  to node  $j$  in

$\Delta t + 1$  steps. Putting these pieces together, we find that the expectation  $\hat{A}$  converges to a concise mathematical form,

$$\begin{aligned} \lim_{T \rightarrow \infty} \hat{A}_{ij}(T) &= \lim_{T \rightarrow \infty} \frac{\tilde{n}_{ij}(T)}{\sum_k \tilde{n}_{ik}(T)} \\ &= \frac{p_i \sum_{\Delta t=0}^{\infty} P(\Delta t) (A^{\Delta t+1})_{ij}}{p_i} \\ &= \sum_{\Delta t=0}^{\infty} P(\Delta t) (A^{\Delta t+1})_{ij}. \end{aligned} \quad (10)$$

Thus far, we have not appealed to our maximum entropy form for  $P(\Delta t)$ . It turns out that doing so allows us to write down an analytic expression for the long-time expectations  $\hat{A}$  simply in terms of the transition structure  $A$  and the inverse temperature  $\beta$ . Noting that  $Z = \sum_{\Delta t=0}^{\infty} e^{-\beta \Delta t} = 1/(1 - e^{-\beta})$  and  $\sum_{\Delta t=0}^{\infty} (e^{-\beta} A)^{\Delta t} = (I - e^{-\beta} A)^{-1}$ , we have

$$\begin{aligned} \hat{A} &= \sum_{\Delta t=0}^{\infty} P(\Delta t) A^{\Delta t+1} \\ &= \frac{1}{Z} A \sum_{\Delta t=0}^{\infty} (e^{-\beta} A)^{\Delta t} \\ &= (1 - e^{-\beta}) A (I - e^{-\beta} A)^{-1}. \end{aligned} \quad (11)$$

This surprisingly simple formula for the representation  $\hat{A}$  is the basis for all of our analytic predictions (Figs. 3c, 3d, and 6b) and is closely related to notions of communicability in complex network theory.<sup>67,68</sup>

**Estimating model parameters and making quantitative predictions.** Given an observed sequence of nodes  $x_1, \dots, x_{t-1}$ , and given an inverse temperature  $\beta$ , our model predicts the anticipation, or expectation, of the subsequent node  $x_t$  to be  $a(t) = \hat{A}_{x_{t-1}, x_t}(t - 1)$ . In order to quantitatively describe the reactions of an individual subject, we must relate the expectations  $a(t)$  to predictions about a person's reaction times  $\hat{r}(t)$  and then calculate the model parameters that best fit the reactions of an individual subject. The simplest possible prediction is given by the linear relation  $\hat{r}(t) = r_0 + r_1 a(t)$ , where the intercept  $r_0$  represents a person's reaction time with zero anticipation and the slope  $r_1$  quantifies the strength with which a person's reaction times depend on their internal expectations.

In total, our predictions  $\hat{r}(t)$  contain three parameters ( $\beta$ ,  $r_0$ , and  $r_1$ ), which must be estimated from the data for each subject. Before estimating these parameters, however, we first regress out the dependencies of each subject's reaction times on the button combinations and trial number using a mixed effects model of the form ' $RT \sim$

$\log(\text{Trial}) * \text{Stage} + \text{Target} + (1 + \log(\text{Trial}) * \text{Stage} | ID)$ . Then, to estimate the model parameters that best describe an individual’s reactions, we minimize the RMS prediction error with respect to each subject’s observed reaction times,  $\text{RMSE} = \sqrt{\sum_t (r(t) - \hat{r}(t))^2}$ . We note that, given a choice for the inverse temperature  $\beta$ , the linear parameters  $r_0$  and  $r_1$  can be calculated analytically using standard linear regression techniques. Thus, the problem of estimating the model parameters can be restated as a one-dimensional minimization problem; that is, minimizing RMSE with respect to the inverse temperature  $\beta$ . To find the global minimum, we began by calculating RMSE along 200 logarithmically-spaced values for  $\beta$  between  $10^{-4}$  and 10. Then, starting at the minimum value of this search, we performed gradient descent until the gradient fell below an absolute value of  $10^{-6}$ . For a derivation of the gradient of the RMSE with respect to the inverse temperature  $\beta$ , we point the reader to the Supplemental Information. Finally, in addition to the gradient descent procedure described above, for each subject we also manually checked the RMSE associated with the two limits  $\beta \rightarrow 0$  and  $\beta \rightarrow \infty$ . The resulting model parameters for all subjects that responded to the modular or lattice graphs are shown in Fig. 4a.

**Experimental setup for serial response tasks.** Subjects performed a self-paced serial reaction time task using a computer screen and keyboard. Each stimulus was presented as a horizontal row of five grey squares; all five squares were shown at all times. The squares corresponded spatially with the keys ‘Space’, ‘H’, ‘J’, ‘K’, and ‘L’, with the left square representing ‘Space’ and the right square representing ‘L’ (Fig. 17b). To indicate a target key or pair of keys for the subject to press, the corresponding squares would become outlined in red (Fig. 17a). When subjects pressed the correct key combination, the squares on the screen would immediately display the next target. If an incorrect key or pair of keys was pressed, the message ‘Error!’ was displayed on the screen below the stimuli and remained until the subject pressed the correct key(s). The order in which stimuli were presented to each subject was prescribed by a random walk on a graph of  $N = 15$  nodes. For each subject, one of the 15 key combinations was randomly assigned to each node in the graph (Fig. 17a). Across all graphs, each node was connected to four other nodes with a uniform 0.25 transition probability. Importantly, given the uniform edge weights and homogeneous node degrees ( $k = 4$ ), the only differences between the transition graphs lay in their higher-order structure.

In the first experiment, we considered two different graph topologies: a *modular* graph with three communities

of five densely-connected nodes and a *lattice* graph representing a  $3 \times 5$  grid with periodic boundary conditions (Fig. 17c). The purpose of this experiment was to demonstrate the systematic dependencies of human reaction times on higher-order network structure, following similar results reported in recent literature.<sup>24,39</sup> In particular, we demonstrate two higher-order network effects: In the *cross-cluster surprisal* effect, average reaction times for within-cluster transitions in the modular graph are significantly faster than reaction times for between-cluster transitions (Fig. 2a); and in the *modular-lattice* effect, average reaction times in the modular graph are significantly faster than reaction times in the lattice graph (Fig. 2b).

In the second experiment, we considered a *ring* graph where each node was connected to its nearest and next-nearest neighbors in the ring (Fig. 6a). In order to study the dependence of human expectations on violations to the network structure, the first 500 trials for each subject constituted a standard random walk, allowing each subject time to develop expectations about the underlying transition structure. Across the final 1000 trials, we randomly distributed 50 network violations: 20 short violations of topological distance two and 30 long violations, 20 of topological distance three and 10 of topological distance four (Fig. 6a). As predicted by our model, we found a novel *violations* effect, wherein violations of longer topological distance give rise to larger increases in reaction times than short, local violations (Figs. 6b and 6c).

**Data analysis for serial response tasks.** To make inferences about subjects' internal expectations based on their reaction times, we used more stringent filtering techniques than previous experiments when pre-processing the data.<sup>24</sup> Across both experiments, we first excluded from analysis the first 500 trials, in which subjects' reaction times varied wildly (Fig. 17e), focusing instead on the final 1000 trials, at which point subjects had already developed internal expectations about the transition structures. We then excluded all trials in which subjects responded incorrectly. Finally, we excluded reaction times that were implausible, either three standard deviations from a subjects' mean reaction time or below 100 ms. Furthermore, when measuring the network effects in both experiments, we also excluded reaction times over 3500 ms for implausibility (Figs. 2 and 6). When learning the parameters of our model and measuring model performance in the first experiment (Fig. 4), to avoid large fluctuations in the results based on outlier reactions, we were even more stringent, excluding all reaction times over 2000 ms. Taken together, when

measuring the cross-cluster surprisal and modular-lattice effects (Fig. 2), we used an average of 931 trials per subject; when learning and evaluating our model (Fig. 4), we used an average of 911 trials per subject; and when measuring the violation effects (Fig. 6), we used an average of 917 trials per subject. To ensure that our results are robust to particular choices in the data processing, we additionally studied all 1500 trials for each subject rather than just the final 1000, confirming that both the cross-cluster surprisal and modular-lattice effects remain significant across all trials (Supplementary Tabs. 9 and 10).

**Measurement of higher-order network effects using mixed effects models.** In order to extract the effects of higher-order network structure on subjects' reaction times, we used linear mixed effects models, which have become prominent in human research where many measurements are made for each subject.<sup>40,69</sup> Put simply, mixed effects models generalize standard linear regression techniques to include both *fixed* effects, which are constant across subjects, and *random* effects, which vary between subjects. Compared with standard linear models, mixed effects models allow for differentiation between effects that are subject-specific and those that persist across an entire population. Here, all models were fit using the `fitlme` function in MATLAB (R2018a), and random effects were chosen as the maximal structure that (i) allowed model convergence and (ii) did not include effects whose 95% confidence intervals overlapped with zero.<sup>70</sup> In what follows, when referring to our mixed effects models, we employ the standard R notation.<sup>71</sup>

First, we considered the cross-cluster surprisal effect (Fig. 2a). Since we were only interested in measuring higher-order effects of the network topology on human reaction times, it was important to regress out simple biomechanical dependencies on the target button combinations (Fig. 17d) and the natural quickening of reactions with time (Fig. 17e). Also, since some subjects responded to both the modular and lattice graphs (see Experimental Procedures), it was important to account for changes in reaction times due to which stage of the experiment a subject was in. To measure the cross-cluster surprisal effect, we fit a mixed effects model with the formula ' $RT \sim \log(Trial)*Stage+Target+Trans\_Type+(1+\log(Trial)*Stage+Trans\_Type | ID)$ ', where  $RT$  is the reaction time,  $Trial$  is the trial number between 501 and 1500 (we found that  $\log(Trial)$  was far more predictive of subjects' reaction times than the trial number itself),  $Stage$  is the stage of the experiment (either one or two),  $Target$

is the target button combination, *Trans.Type* is the type of transition (either within-cluster or between-cluster), and *ID* is each subject's unique ID. Learning this mixed effects model (Supplementary Tab. 1), we found a fixed 50 ms increase in reaction times ( $p < 0.001$ ) for between-cluster transitions relative to within-cluster transitions (Fig. 2a). This increase indicates that the subjects had systematically stronger expectations for within-cluster transitions than for between-cluster transitions. Before proceeding, we note that because reaction times are not Gaussian distributed, it is fairly standard to perform a log transformation. However, for the above result as well as those that follow, we find the same qualitative effects with or without a log transformation.

We next studied the modular-lattice effect (Fig. 2b). To do so, we fit a mixed effects model with the formula ' $RT \sim \log(Trial) * Stage + Target + Graph + (1 + \log(Trial) * Stage + Graph | ID)$ ', where *Graph* represents the type of transition network, either modular or lattice. Learning this mixed effects model (Supplementary Tab. 2), we found a fixed 31 ms increase in reaction times ( $p < 0.001$ ) in the lattice graph relative to the modular graph (Fig. 2b). This increase indicates that subjects had systematically stronger expectations overall for transitions in the modular graph than in the lattice graph, again suggesting that densely-connected communities conserve probability weight in mental estimates of transition structures.

Finally, we considered the effects of violations of varying topological distance in the ring lattice (Fig. 6c). We fit a mixed effects model with the formula ' $RT \sim \log(Trial) + Target + Recency + Top\_Dist + (1 + \log(Trial) + Recency + Top\_Dist | ID)$ ', where *Recency* represents the number of trials since last observing a node and *Top\_Dist* represents the topological distance of a transition, either one for a standard transition, two for a short violation, or three for a long violation. We included *Recency* in the model to ensure that any dependence on topological distance was purely due to internal expectations about the transition structure and not merely the result of recency effects.<sup>63</sup> Learning the model (Supplementary Tabs. 7 and 8), we found a 38 ms increase in reaction times for short violations relative to standard transitions ( $p < 0.001$ ), a 63 ms increase in reaction times for long violations relative to standard transitions ( $p < 0.001$ ), and a 28 ms increase in reaction times for long violations relative to short violations ( $p = 0.011$ ). Together, these results indicate that, even after accounting for recency effects, people's expectations of network violations decrease with increasing topological distance. Put simply, people are more surprised by violations to the

network structure that take them further from their current position in the network, suggesting that people have an implicit understanding of the topological distances between nodes in the network.

**Experimental setup for  $n$ -back memory task.** Subjects performed a series of  $n$ -back memory tasks using a computer screen and keyboard. Each subject observed a random sequence of the letters ‘B’, ‘D’, ‘G’, ‘T’, and ‘V’, wherein each letter was randomly displayed in either upper or lower case. The subjects responded on each trial using the keyboard to indicate whether or not the current letter was the same as the letter that occurred  $n$  trials previously. For each subject, this task was repeated for the conditions  $n = 1, 2$ , and  $3$ , and each condition consisted of a sequence of 100 letters. The three conditions were presented in a random order to each subject. After the  $n$ -back task, each subject then performed a serial response task (as described above) consisting of 1500 trials drawn from the modular graph.

**Data analysis for  $n$ -back memory task.** In order to estimate the inverse temperature  $\beta$  for each subject from their  $n$ -back data, we directly measured their memory distribution  $P(\Delta t)$ . As described in the main text, we treated each positive response indicating that the current stimulus matched the target stimulus as a sample of  $P(\Delta t)$  by measuring the distance in trials  $\Delta t$  between the last instance of the current stimulus and the target (Fig. 5a). For each subject, we combined all such samples across the three conditions  $n = 1, 2$ , and  $3$  to arrive at a histogram for  $\Delta t$ . In order to generate robust estimates for the inverse temperature  $\beta$ , we generated 1000 bootstrap samples of the  $\Delta t$  histogram for each subject. For each sample, we calculated a linear fit to the distribution  $P(\Delta t)$  on log-linear axes within the domain  $0 \leq \Delta t \leq 4$  (note that we could not carry the fit out to  $\Delta t = 10$  because the data is much sparser for individual subjects). To ensure that the logarithm of  $P(\Delta t)$  was well defined for each sample – that is, to ensure that  $P(\Delta t) > 0$  for all  $\Delta t$  – we added one count to each value of  $\Delta t$ . We then estimated the inverse temperature  $\beta$  for each sample by calculating the negative slope of the linear fit of  $\log P(\Delta t)$  versus  $\Delta t$ . To arrive at an average estimate of  $\beta$  for each subject, we averaged  $\beta$  across the 1000 bootstrap samples. Finally, we compared these estimates of  $\beta$  from the  $n$ -back experiment with estimates of  $\beta$  from subjects’ reaction times in the subsequent serial response task, as described above. We found that these two independent estimates of people’s inverse temperatures are significantly correlated (excluding subjects for which  $\beta = 0$  or  $\beta \rightarrow \infty$ ), with a Spearman coefficient  $r_s = 0.28$  ( $p = 0.047$ ).

**Experimental procedures.** All participants provided informed consent in writing and experimental methods were

approved by the Institutional Review Board of the University of Pennsylvania. In total, we recruited 604 unique participants to complete our studies on Amazon's Mechanical Turk. For the first serial response experiment, 101 participants only responded to sequences drawn from the modular graph, 113 participants only responded to sequences drawn from the lattice graph, and 72 participants responded to sequences drawn from both the modular and lattice graphs in back-to-back (counter-balanced) sessions for a total of 173 exposures to the modular graph and 185 exposures to the lattice graph. For the second serial response experiment, we recruited 78 participants to respond to sequences drawn from the ring graph with violations randomly interspersed. For the  $n$ -back experiment, 150 subjects performed the  $n$ -back task and, of those, 88 completed the subsequent serial response task. Finally, we recruited 90 subjects to perform our Hamiltonian walk experiment, as described in the Supplementary Information. Worker IDs were used to exclude duplicate participants between experiments, and all participants were financially remunerated for their time. In the first experiment, subjects were paid up to \$11 for up to an estimated 60 minutes: \$3 per network for up to two networks, \$2 per network for correctly responding on at least 90% of the trials, and \$1 for completing the entire task. In the second experiment, subjects were paid up to \$7.50 for an estimated 30 minutes: \$5.50 for completing the experiment and \$2 for correctly responding on at least 90% of the trials. In the  $n$ -back experiment, subjects were paid up to \$8.50 for an estimated 45 minutes: \$7 for completing the entire experiment and \$1.50 for correctly responding on at least 90% of the serial response trials.

At the beginning of each experiment, subjects were provided with the following instructions: "In a few minutes, you will see five squares shown on the screen, which will light up as the experiment progresses. These squares correspond with keys on your keyboard, and your job is to watch the squares and press the corresponding key when that square lights up." For the 72 subjects that responded to both the modular and lattice graphs, an additional piece of information was also provided: "This part will take around 30 minutes, followed by a similar task which will take another 30 minutes." Before each experiment began, subjects were given a short quiz to verify that they had read and understood the instructions. If any questions were answered incorrectly, subjects were shown the instructions again and asked to repeat the quiz until they answered all questions correctly. Next, all subjects were shown a 10-trial segment that did not count towards their performance; this segment also displayed text on the screen explicitly telling



the subject what keys to press on their keyboard. Subjects then began their 1500-trial experiment. For the subjects that responded to both the modular and lattice graphs, a brief reminder was presented before the second graph, but no new instructions were given. After completing each experiment, subjects were presented with performance information and their bonus earned, as well as the option to provide feedback.

## **Data Availability**

The data that support the findings of this study are available from the corresponding author upon request.

**Acknowledgements** We thank Nathaniel Nyema for help performing the experiments, and we thank Pedro Ortega for inspiring our use of the free energy principle. D.S.B., C.W.L., and A.E.K. acknowledge support from the John D. and Catherine T. MacArthur Foundation, the Alfred P. Sloan Foundation, the ISI Foundation, the Paul Allen Foundation, the Army Research Laboratory (W911NF-10-2-0022), the Army Research Office (Bassett-W911NF-14-1-0679, Grafton-W911NF-16-1-0474, DCIST- W911NF-17-2-0181), the Office of Naval Research, the National Institute of Mental Health (2-R01-DC-009209-11, R01-MH112847, R01-MH107235, R21-MH-106799), the National Institute of Child Health and Human Development (1R01HD086888-01), National Institute of Neurological Disorders and Stroke (R01 NS099348), and the National Science Foundation (BCS-1441502, BCS-1430087, NSF PHY-1554488 and BCS-1631550). The content is solely the responsibility of the authors and does not necessarily represent the official views of any of the funding agencies.

**Author contributions** C.W.L., A.E.K., and D.S.B. conceived the project. C.W.L. designed the model and performed the analysis. C.W.L., A.E.K., and D.S.B. planned the experiments and discussed the results.

A.E.K. performed the experiments. C.W.L. wrote the manuscript and Supplementary Information. A.E.K. and D.S.B. edited the manuscript and Supplementary Information.

**Competing interests** The authors declare no competing financial interests.

**Corresponding author** Correspondence and requests for materials should be addressed to D.S.B. (dsb@seas.upenn.edu).

**Supplementary information** Supplementary text and figures accompany this paper.

## **Structure from noise: Mental errors yield abstract representations of events**

### *Supplementary Information*

In this Supplementary Information, we provide extended discussion and data to support the results presented in the main text. The content is organized to roughly mirror the organization of the paper:

1. We begin by presenting experimental evidence showing that human reaction times – in addition to depending on higher-order network features – also reflect differences in the fine-scale structure at the level of individual nodes. Just as for the higher-order effects presented in the main text, we demonstrate that these fine-scale phenomena are accurately predicted by our maximum entropy model.
2. To facilitate the reproducibility of our main results, we present the mixed effects models that were used to measure the cross-cluster surprisal and modular-lattice effects.
3. To establish that these higher-order effects cannot simply be explained by recency, we present a new experiment that includes trials from Hamiltonian walks.
4. We show that the probability of an error on the the serial response tasks increases for between- versus within-cluster transitions in the modular graph, indicating that our framework can be used to predict more than just human reaction times.
5. We present the mixed effects models that were used to measure the effects of violations in the ring graph.

6. We show that the cross-cluster surprisal and modular-lattice effects persist even if we consider all 1500 trials for each subject, suggesting that our main experimental results are robust to the particulars of our data processing.
7. We provide a simple and intuitive argument that the forgetting of past stimuli altogether cannot explain the higher-order network effects that we examine in the main text.
8. To aid in the reconstruction of our gradient descent algorithm for estimating the inverse temperature  $\beta$  from subjects' reaction times, we derive an analytic form for the gradient of the RMS prediction error of our model with respect to  $\beta$ .
9. Finally, we highlight the relation between our model and the successor representation in reinforcement learning, describing both mathematical similarities and conceptual differences.

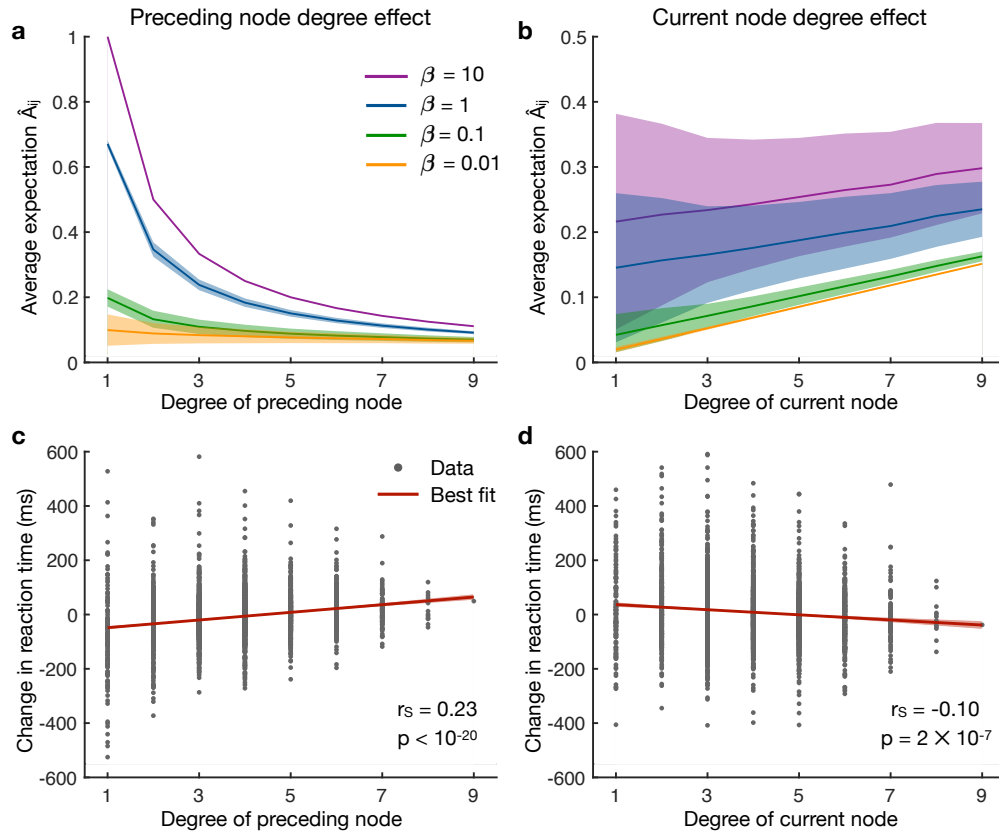
## **1 The effects of node heterogeneity on human expectations**

In the main text, we demonstrated that human expectations depend critically on the higher-order network structure of transitions. In addition to these higher-order phenomena, it has long been known that human expectations also reflect differences in the fine-scale structure of transition networks.<sup>6,24</sup> For instance, humans are surprised by rare transitions, represented in a transition network by edges with low probability weight.<sup>4</sup> Here, we provide empirical evidence showing that people's expectations also depend on the local topologies of the nodes that bookend a transition, and that these fine-scale effects are consistently predicted by our maximum entropy model.

In order to clearly study the effects of higher-order network structure, in the main text we

focused on networks with uniform edge weights and node degrees. Here, to study the effects of node heterogeneity, we instead consider a set of Erdős-Rényi random graphs with the same number of nodes ( $N = 15$ ) and edges (30) as in our previous modular and lattice graphs. To ensure that the random walks are properly defined, we set the transition probability  $A_{ij}$  of each edge in the graph to  $1/d_i$ , where  $d_i$  is the degree of node  $i$ . Since the probabilities  $A_{ij}$  decrease as the degree  $d_i$  increases, one should suspect that high-degree (or hub) nodes yield decreased anticipations – and therefore increased reaction times – at the next step of a random sequence. Indeed, using Eq. (6) from the main text, we find that our model analytically predicts decreased expectations following a high-degree node (Supplementary Fig. 7a). Furthermore, across 177 human subjects, we find a strong positive correlation between people’s reaction times and the degree of the preceding node in the sequence (Supplementary Fig. 7b).

Interestingly, while people’s anticipations exhibit a sharp decline if the preceding node has high-degree, our model predicts that these hub nodes instead yield increased anticipations on the current step (Supplementary Fig. 7c). Thus, while hub nodes give rise to marked increases in reaction times on the subsequent step, these high-degree nodes actually yield faster reactions on the current step<sup>24</sup> (Supplementary Fig. 7d). This juxtaposition of effects from one time step to the next highlights the complex ways in which the network structure of transitions can affect people’s mental representations. Additionally, the success of our model in predicting these competing phenomena further strengthens our conclusion that mental errors play a crucial role in shaping people’s internal expectations.



**Supplementary Fig. 1: The effects of node degree on reaction times.**

**a**, The average expectation  $\hat{A}_{ij}$  plotted with respect to the degree of the preceding node  $i$  across a range of inverse temperatures  $\beta$ . As expected, expectations decrease as the degree of the preceding node increases; and for  $\beta = 10$ , we have  $\hat{A}_{ij} \approx A_{ij} = 1/d_i$ . The lines and shaded regions represent averages and 95% confidence intervals over 1000 randomly-generated Erdős-Rényi networks. **b**, People exhibit sharp increases in reaction time following nodes of higher degree, with Spearman's correlation  $r_s = 0.23$ . The data is combined across 177 subjects, each of whom was asked to respond to a sequence of 1500 stimuli drawn from a random Erdős-Rényi network. Each data point represents the average reaction time for one node of a graph, and so each subject contributes 15 points. The line and shaded region represent the best fit and 95% confidence interval, respectively. **c**, The average expectation  $\hat{A}_{ij}$  plotted with respect to the degree of the current node  $j$  across the same range of inverse temperatures as in **a**. **d**, People exhibit a steady decline in reaction times as the current node degree increases, with Spearman's correlation  $r_s = -0.10$ .

## 2 Measuring higher-order network effects

In order to extract the effects of higher-order network structure on subjects' reaction times, we use linear mixed effects models, which have become prominent in human research where many measurements are made for each subject.<sup>40,69</sup> To fit our mixed effects models and to estimate the statistical significance of each effect we use the `fitlme` function in MATLAB (R2018a). In what follows, when referring to our mixed effects models, we adopt the standard R notation.<sup>71</sup>

**Cross-cluster surprisal effect.** We first measure the cross-cluster surprisal effect (Fig. 2a) using a mixed effects model with the formula ' $RT \sim \log(Trial) * Stage + Target + Trans\_Type + (1 + \log(Trial) * Stage + Trans\_Type | ID)$ ', where  $RT$  is the reaction time,  $Trial$  is the trial number between 501 and 1500,  $Stage$  is the stage of the experiment (either one or two),  $Target$  is the target button combination,  $Trans\_Type$  is the type of transition (either within-cluster or between-cluster), and  $ID$  is each subject's unique ID. This mixed effects model is summarized in Supplementary Tab. 1, reporting a 50 ms increase in reaction times for between-cluster transitions relative to within-cluster transitions (Fig. 2a).

**Modular-lattice effect.** We next measure the modular-lattice effect (Fig. 2b) using a mixed effects model of the form ' $RT \sim \log(Trial) * Stage + Target + Graph + (1 + \log(Trial) * Stage + Graph | ID)$ ', where  $Graph$  represents the type of transition network, either modular or lattice. This mixed effects model is summarized in Supplementary Tab. 2, reporting a 31 ms increase in reaction times in the lattice graph relative to the modular graph (Fig. 2b).

Effect	Estimate (ms)	t-value	Pr(> t )	Significance
(Intercept)	1528.3 ± 78.1	19.56	< 0.001	***
log(Trial)	-101.3 ± 9.6	-10.50	< 0.001	***
Stage	-708.2 ± 95.0	-7.45	< 0.001	***
Trans_Type	49.7 ± 6.3	7.94	< 0.001	***
log(Trial):Stage	78.9 ± 11.9	6.63	< 0.001	***

**Supplementary Tab. 1: Mixed effects model measuring the cross-cluster surprisal effect.** A mixed effects model fit to the reaction time data for the modular graph with the goal of measuring the cross-cluster surprisal effect. We find a significant 50 ms increase in reaction times for between-cluster transitions versus within-cluster transitions (grey). The significance column represents  $p$ -values less than 0.001 (\*\*\*), less than 0.01 (\*\*), and less than 0.05 (\*).

Effect	Estimate (ms)	t-value	Pr(> t )	Significance
(Intercept)	1467.3 ± 49.0	29.96	< 0.001	***
log(Trial)	-98.4 ± 6.2	-15.96	< 0.001	***
Stage	-588.3 ± 60.4	-9.74	< 0.001	***
Graph	31.4 ± 5.9	5.36	< 0.001	***
log(Trial):Stage	75.3 ± 8.5	8.83	< 0.001	***

**Supplementary Tab. 2: Mixed effects model measuring the modular-lattice effect.** A mixed effects model fit to the reaction time data for the modular and lattice graphs with the goal of measuring the modular-lattice effect. We find a significant 31 ms increase in reaction times overall in the lattice graph relative to the modular graph (grey). The significance column represents  $p$ -values less than 0.001 (\*\*\*), less than 0.01 (\*\*), and less than 0.05 (\*).



### 3 Controlling for recency: Cross cluster surprisal in Hamiltonian walks

Throughout the main text, we assume that people’s reaction times reflect their internal representations of the transition structure. To justify this assumption, we must show that the higher-order network effects cannot simply be explained by recency. To control for recency effects, we employ the concept of a Hamiltonian walk, which is a walk through the transition graph that visits each node exactly once. We run a new experiment in which each subject is presented with a sequence of 1500 stimuli drawn from the modular graph: The first 700 nodes reflect a standard random walk, while the remaining 800 trials consist of 8 repeated segments of 85 stimuli specified by a random walk followed by 15 stimuli specified by a Hamiltonian walk. The initial 700 random walk trials are meant to constitute a learning phase in which the subject builds an internal representation of the modular graph. Since, in the modular graph, Hamiltonian walks do not obey the same transition probabilities as random walks, the sequences of 85 random walk trials between each Hamiltonian sequence are meant to help the subject maintain their learned representation. Within the set of Hamiltonian walks through the modular graph, the probability of transitioning from one cluster boundary node to the adjacent one (if not already visited) is 1, whereas the probability of transitioning from the latter boundary node to each of the adjacent non-boundary nodes is  $1/3$ . To eliminate this difference, we randomly selected one fixed Hamiltonian walk for each subject. This fixed walk was entered at a different node depending on where the preceding walk terminated, and we randomly switched between forward and backward traversals for each walk.<sup>22</sup>

We measure the cross-cluster surprisal within the Hamiltonian trials using a mixed effects

Effect	Estimate (ms)	t-value	Pr(> t )	Significance
(Intercept)	1601.7 ± 207.8	7.71	< 0.001	***
log(Trial)	-124.7 ± 28.4	-4.38	< 0.001	***
Trans_Type	25.1 ± 9.4	2.68	0.007	**

**Supplementary Tab. 3: Mixed effects model measuring the cross-cluster surprisal effect in Hamiltonian walks.** A mixed effects model fit to subjects' reaction times in Hamiltonian walks on the modular graph with the goal of measuring the cross-cluster surprisal effect. We find a significant 25 ms increase in reaction times for between-cluster transitions versus within-cluster transitions (grey). The significance column represents  $p$ -values less than 0.001 (\*\*\*), less than 0.01 (\*\*), and less than 0.05 (\*).

model with the formula ' $RT \sim \log(Trial) + Target + Trans\_Type + (1 + \log(Trial)|ID)$ ', where each of the variables has been defined previously. Note that we have removed the mixed effect on the  $Trans\_Type$  variable because, when it was included, its estimate overlapped significantly with zero. The model is summarized in Supplementary Tab. 3, reporting a 25 ms increase in reaction times for between-cluster transitions relative to within-cluster transitions within Hamiltonian trials ( $p = 0.007$ ). This result demonstrates conclusively that the cross-cluster surprisal effect cannot be explained by recency alone, and must therefore must be at least partially driven by people's internal representations of the transition structure.

As discussed above, the first 700 trials of each sequence were drawn from a random walk to allow subjects to build an internal representation of the transition structure. Since the transition probabilities reflected in the Hamiltonian walks differ from those in the random walks, we then expect subjects' representations to shift as they observe Hamiltonian trials. Therefore, to further

Effect	Estimate (ms)	t-value	Pr(> t )	Significance
(Intercept)	1466.8 ± 217.5	6.74	< 0.001	***
log(Trial)	-105.5 ± 29.9	-3.53	< 0.001	***
Trans_Type	691.56 ± 318.23	2.17	0.030	*
log(Trial):Trans_Type	-94.9 ± 45.3	-2.10	0.036	*

**Supplementary Tab. 4: Mixed effects model measuring the decrease in cross-cluster surprisal with increasing Hamiltonian trials.** A mixed effects model fit to subjects' reaction times in Hamiltonian walks on the modular graph with the goal of measuring the dependence of the cross-cluster surprisal on increasing Hamiltonian trials. We find a significant decrease in the strength of the cross-cluster surprisal with increasing Hamiltonian trials (grey). The significance column represents  $p$ -values less than 0.001 (\*\*\*), less than 0.01 (\*\*), and less than 0.05 (\*).

establish the notion that people's reactions are primarily driven by their internal representations, here we show that the strength of the cross-cluster surprisal decreases as subjects observe increasing numbers of Hamiltonian trials. To do so, we use a mixed effects model with the formula ' $RT \sim \log(Trial) * Trans\_Type + Target + (1 + \log(Trial)|ID)$ ', where the only difference with the formula above is that here we include an interaction term between  $\log(Trial)$  and  $Trans\_Type$ . The results of the fitted model are summarized in Supplementary Tab. 4, reporting a significant decrease in the strength of the cross-cluster surprisal with increasing Hamiltonian trials ( $p = 0.036$ ).

**Experimental setup and procedures.** Subjects performed a self-paced serial reaction time task, as described in the Methods section of the main text. The only difference between this experiment

and that described previously is that the 1500 trials were split into 700 trials drawn as a random walk and a subsequent 800 trials divided into 8 segments of 85 random walk trials followed by 15 Hamiltonian walk trials, all drawn from the modular graph. In total, we recruited 90 subjects to perform this Hamiltonian walk experiment, and they were paid up to \$5 each for an estimated 30 minutes: \$3.50 for completing the task and \$1.50 for correctly responding on at least 90% of the trials.

#### 4 Network effects on error trials

Thus far we have focused on predicting human reaction times as a proxy for people’s anticipations of transitions. Another way to probe anticipation is by studying the trials on which subjects respond incorrectly; one might expect that the probability of an erroneous response should increase with decreasing anticipation. Here, we test this hypothesis for between- versus within-cluster transitions in the modular graph and for all transitions in the modular graph versus the lattice graph.

**Cross-cluster surprisal effect on errors.** First, we consider the cross-cluster surprisal effect on errors defined by an increase in task errors for transitions between clusters relative to transitions within clusters in the modular graph. We employ a mixed effects model with formula ‘ $Error \sim \log(Trial) + Stage + Target + Trans_{Type} + (1 + \log(Trial) + Stage + Trans_{Type}|ID)$ ’, where *Error* indicates whether the subject provided an incorrect (‘1’) or correct (‘0’) response, *Trial* is the trial number between 501 and 1500, *Stage* is the stage of the experiment (either one or two), *Target* is the target button combination, *Trans\_Type* is the type of transition (either

Effect	Estimate	t-value	Pr(> t )	Significance
(Intercept)	0.010 ± 0.011	0.86	0.390	
log(Trial)	0.004 ± 0.002	2.11	0.035	*
Stage	0.011 ± 0.007	1.59	0.112	
Trans_Type	0.008 ± 0.002	3.32	< 0.001	***

**Supplementary Tab. 5: Mixed effects model measuring the cross-cluster effect on task errors.** A mixed effects model fit to predict error trials for the modular graph with the goal of measuring the cross-cluster effect on task errors. We find a significant increase in task errors for between-cluster transitions relative to within-cluster transitions (grey). The significance column represents  $p$ -values less than 0.001 (\*\*\*), less than 0.01 (\*\*), and less than 0.05 (\*).

within-cluster or between-cluster), and  $ID$  is each subject’s unique ID. Note that, relative to our measurement of the cross-cluster surprisal for reaction times, we have removed the interaction between  $\log(Trial)$  and  $Stage$  because it was not statistically significant in this setting. We find a significant increase in errors for between- versus within-cluster transitions (Supplementary Tab. 5), suggesting yet again that subjects have weaker anticipation for cross-cluster transitions than for within-cluster transitions.

**Modular-lattice effect on errors.** Second, we consider the modular-lattice effect on errors defined by an increase in task errors for the lattice graph relative to the modular graph. We employ a mixed effects model with formula ‘ $Error \sim \log(Trial) + Stage + Target + Graph + (1 + \log(Trial) + Stage + Graph|ID)$ ’, where each of the variables has been defined previously. We again note that we have removed the interaction between  $\log(Trial)$  and  $Stage$  because it was

Effect	Estimate	t-value	Pr(> t )	Significance
(Intercept)	0.031 ± 0.009	3.58	< 0.001	* * *
log(Trial)	0.002 ± 0.001	1.42	0.156	
Stage	0.001 ± 0.002	0.33	0.739	
Graph	0.001 ± 0.002	0.11	0.916	

**Supplementary Tab. 6: Mixed effects model measuring the modular-lattice effect on task errors.** A mixed effects model fit to predict error trials for the modular and lattice graphs with the goal of measuring the modular-lattice effect on task errors. We do not find a significant increase in errors for either graph (grey). The significance column represents  $p$ -values less than 0.001 (\* \* \*), less than 0.01 (\*\*), and less than 0.05 (\*).

not statistically significant in our prediction of task errors. Inspecting the mixed effects model described in Supplementary Tab. 6, we do not find a significant difference in the number of task errors between the modular and lattice graphs. One possible explanation for this lack of an effect is that people’s task accuracy is predominantly impacted by very poorly anticipated transitions. Thus, while anticipation in the lattice graph is lower than that in the modular graph on average, it could be the case that the significant decrease in anticipation for cross-cluster transitions in the modular graph yields a similar number of task errors overall.

## 5 Measuring the effects of network violations.

We study the effects of violations of varying topological distance in the ring graph using a mixed effects model with the formula ‘ $RT \sim \log(Trial) + Target + Recency + Top\_Dist + (1 +$

Effect	Estimate (ms)	t-value	Pr(> t )	Significance
(Intercept)	1352.7 ± 79.2	17.07	< 0.001	***
log(Trial)	-101.1 ± 10.2	-9.96	< 0.001	***
Recency	2.1 ± 0.1	16.20	< 0.001	***
Top_Dist (short vs. no violation)	37.9 ± 8.4	4.50	< 0.001	***
Top_Dist (long vs. no violation)	63.3 ± 7.8	8.07	< 0.001	***

**Supplementary Tab. 7: Mixed effects model measuring the effects of violations relative to standard transitions.** A mixed effects model fit to the reaction time data for the ring graph with the goal of measuring the effects of violations relative to standard transitions. We find a significant increase in reaction times of 38 ms for short violations and 63 ms for long violations (grey), even after accounting for recency effects. The significance column represents  $p$ -values less than 0.001 (\*\*\*), less than 0.01 (\*\*), and less than 0.05 (\*).

$\log(\text{Trial}) + \text{Recency} + \text{Top\_Dist} | ID)$ , where *Recency* represents the number of trials since last observing a node<sup>63</sup> and *Top\_Dist* represents the topological distance of a transition, either one for a standard transition, two for a short violation, or three for a long violation. The results of fitting this mixed effects model are summarized in Supplementary Tab. 7, reporting increases in reaction times over standard transitions of 38 ms for short violations and 63 ms for long violations. Second, to measure the difference in reaction times between long and short violations, we implemented a model of the same form, but restricted *Top\_Dist* to only include short violations of topological distance two and long violations of topological distances three and four. This model is summarized in Supplementary Tab. 8, reporting a 28 ms increase in reaction times for long violations relative to short violations.

Effect	Estimate (ms)	t-value	Pr(> t )	Significance
(Intercept)	1380.9 ± 156.1	8.84	< 0.001	***
log(Trial)	-97.1 ± 21.3	-4.57	< 0.001	***
Recency	0.7 ± 0.3	2.67	0.008	**
Top_Dist (long vs. short violation)	28.4 ± 11.2	2.54	0.011	*

**Supplementary Tab. 8: Mixed effects model measuring the effects of long versus short violations.** A mixed effects model fit to the reaction time data for the ring graph with the goal of measuring the effects of long versus short violations. We find a significant 28 ms increase in reaction times for long violations relative to short violations (grey), even after accounting for recency effects. The significance column represents  $p$ -values less than 0.001 (\*\*\*), less than 0.01 (\*\*), and less than 0.05 (\*).

## 6 Measuring network effects including early trials

Throughout the above analysis of the serial response tasks, we purposefully omitted the first 500 trials for each subject, choosing instead to focus on the final 1000 trials. We did this in order to allow the subjects to build an internal representation of each network structure before probing their anticipations of transitions. Here, we show that this data processing step is not necessary to observe higher-order network effects; that is, we show that there exist significant network effects even if we include the first 500 trials in our analysis.

**Cross-cluster surprisal effect.** We first consider the cross-cluster surprisal effect defined by an increase in reaction times for transitions between clusters relative to transitions within clusters in the modular graph. Using a mixed effects model of the same form as that used in the previous



Effect	Estimate (ms)	t-value	Pr(> t )	Significance
(Intercept)	1427.0 ± 47.9	29.81	< 0.001	***
log(Trial)	-88.4 ± 5.1	-17.34	< 0.001	***
Stage	-643.7 ± 57.0	-11.29	< 0.001	***
Trans_Type	51.9 ± 6.2	8.41	< 0.001	***
log(Trial):Stage	69.1 ± 12.1	12.07	< 0.001	***

**Supplementary Tab. 9: Mixed effects model measuring the cross-cluster surprisal effect including the first 500 trials.** A mixed effects model fit to all of the reaction time data, including the first 500 trials for each subject, for the modular graph with the goal of measuring the cross-cluster surprisal effect. We find a significant 52 ms increase in reaction times for between-cluster transitions versus within-cluster transitions. The significance column represents  $p$ -values less than 0.001 (\*\*\*), less than 0.01 (\*\*), and less than 0.05 (\*).

analysis (i.e., ‘ $RT \sim \log(\text{Trial}) * \text{Stage} + \text{Target} + \text{Trans\_Type} + (1 + \log(\text{Trial}) * \text{Stage} + \text{Trans\_Type} | ID)$ ’), and including all 1500 trials for each subject, we find a significant 52 ms increase in reaction times for between- versus within-cluster transitions (Supplementary Tab. 9). We note that this effect is even larger than that observed in our previous analysis (Supplementary Tab. 1).

**Modular-lattice effect.** We next consider the modular-lattice effect defined by an increase in reaction times in the lattice graph relative to the modular graph. Using a mixed effects model of the same form as that used in the previous analysis (i.e., ‘ $RT \sim \log(\text{Trial}) * \text{Stage} + \text{Target} + \text{Graph} + (1 + \log(\text{Trial}) * \text{Stage} + \text{Graph} | ID)$ ’), and including all 1500 trials for each subject,

Effect	Estimate (ms)	t-value	Pr(> t )	Significance
(Intercept)	1377.6 ± 30.6	45.07	< 0.001	***
log(Trial)	-87.3 ± 3.4	-25.82	< 0.001	***
Stage	-511.1 ± 25.6	-19.94	< 0.001	***
Graph	27.2 ± 5.8	4.69	< 0.001	***
log(Trial):Stage	64.4 ± 3.6	18.15	< 0.001	***

**Supplementary Tab. 10: Mixed effects model measuring the modular-lattice effect including the first 500 trials.** A mixed effects model fit to all of the reaction time data, including the first 500 trials for each subject, for the modular and lattice graphs with the goal of measuring the modular-lattice effect. We find a significant 27 ms increase in reaction times overall in the lattice graph relative to the modular graph. The significance column represents  $p$ -values less than 0.001 (\*\*\*), less than 0.01 (\*\*), and less than 0.05 (\*).

we find a significant 27 ms increase in reaction times in the lattice versus the modular graph (Supplementary Tab. 10). These results demonstrate that higher-order network effects studied in the main text exist throughout the entire serial response task.

## 7 The simple forgetting of stimuli cannot explain network effects

In the derivation of our model, the central mathematical object is the memory distribution  $P(\Delta t)$ , which represents the probability that a person recalls the stimulus that occurred at time  $t - \Delta t$  instead of the stimulus that they were trying to recall at time  $t$ . Generally, this memory distribution is intended to reflect the erroneous shuffling of past stimuli in a person's memory. Alternatively, one could imagine errors in memory that reflect the forgetting of past stimuli altogether, a process

that has recently been shown to impact human reinforcement learning<sup>55,56</sup> and to facilitate flexible and generalizable decision making<sup>47</sup>. Here we argue that this second form of cognitive errors – that is, the simple forgetting of stimuli – cannot explain the higher-order network effects described in the main text.

Consider a sequence of stimuli reflecting a random walk of length  $T$  on a network defined by the transition matrix  $A$ , where  $A_{ij}$  represents the probability of transitioning from stimulus  $i$  to stimulus  $j$ . Given a running tally  $n_{ij}(T)$  of the number of times each transition has occurred, we recall that the most accurate prediction for the transition structure is given by the maximum likelihood estimate  $\hat{A}_{ij}^{\text{MLE}}(T) = n_{ij}(T) / \sum_k n_{ik}(T)$ . Now suppose that a human learner forgets each observed transition at some fixed rate. On average, this process of estimating  $A$  after forgetting some number of transitions uniformly at random is equivalent to estimating  $A$  at some prior time  $T_{\text{eff}}$ . In other words, forgetting observed transitions at random simply introduces additional white noise into the transitions estimates  $\hat{A}_{ij}^{\text{MLE}}(T)$ . As discussed in the main text, maximum likelihood estimation provides an unbiased estimate of the transition structure, and therefore cannot explain the fact that people’s representations depend systematically on higher-order network organization. Similarly, the addition of white noise to  $\hat{A}_{ij}^{\text{MLE}}(T)$  will also yield an unbiased (although less accurate) estimate of the transition structure. Therefore, while the forgetting of past stimuli certainly plays an important role in a number of cognitive processes<sup>47,55,56</sup>, this mechanism cannot be used to explain the higher-order network effects observed in human experiments and predicted by our model.

## 8 Gradient of RMS error with respect to inverse temperature $\beta$

Given a sequence of nodes  $x_t$ , we recall that our prediction for the reaction time at time  $t$  is given by  $\hat{r}(t) = r_0 + r_1 a(t)$ , where  $a(t) = \hat{A}_{x_{t-1}, x_t}(t-1)$  is the predicted anticipation of node  $x_t$ . The gradient of the RMS error  $\text{RMSE} = \sqrt{\sum_t (r(t) - \hat{r}(t))^2}$  with respect to the inverse temperature  $\beta$  is given by

$$\frac{\partial \text{RMSE}}{\partial \beta} = \frac{r_1}{\text{RMSE}} \sum_t (r(t) - \hat{r}(t)) \frac{\partial a(t)}{\partial \beta}, \quad (12)$$

where the derivative of the anticipation is given by

$$\frac{\partial \hat{A}_{ij}(t)}{\partial \beta} = \frac{1}{\sum_k \tilde{n}_{ik}(t)} \left( \frac{\partial \tilde{n}_{ij}(t)}{\partial \beta} - \hat{A}_{ij} \sum_\ell \frac{\partial \tilde{n}_{i\ell}(t)}{\partial \beta} \right). \quad (13)$$

Recalling Eq. (8) from the main text, the derivative of the transition counts can be written

$$\frac{\partial \tilde{n}_{ij}(t)}{\partial \beta} = \sum_{t'=1}^{t-1} \sum_{\Delta t=0}^{t'-1} \frac{\partial P_{t'}(\Delta t)}{\partial \beta} [i = x_{t'-\Delta t}] [j = x_{t'+1}], \quad (14)$$

where  $P_{t'}(\Delta t)$  represents the probability of accidentally remembering the node  $x_{t'-\Delta t}$  instead of the target node  $x_{t'}$ . Taking one more derivative, we have

$$\frac{\partial P_{t'}(\Delta t)}{\partial \beta} = P_{t'}(\Delta t) \left( -\Delta t + \sum_{\Delta t'=0}^{t'-1} P_{t'}(\Delta t') \Delta t' \right). \quad (15)$$

Taken together, Eqs. (12)-(15) define the derivative of the RMS error with respect to the inverse temperature  $\beta$ , thus completing the description of our gradient descent algorithm.

## 9 Connection to the successor representation

In the limit of an infinitely-long sequence of nodes, we showed in the main text that the transition estimates in our model take the following concise analytic form,

$$\hat{A} = (1 - e^{-\beta})A(I - e^{-\beta}A)^{-1}, \quad (16)$$

where  $A$  is the true transition structure,  $\beta$  is the inverse temperature in our memory distribution, and  $I$  is the identity matrix. Interestingly, this equation takes a similar form to the successor representation from reinforcement learning,

$$M = A(I - \gamma A)^{-1}, \quad (17)$$

where  $\gamma$  is the future discount factor, which tunes the desired time-scale over which a person wishes to make predictions.<sup>58,72</sup> Put simply, starting at some node  $i$ , the successor representation  $M_{ij}$  counts the future discounted occupancy of node  $j$ . Identifying  $\gamma = e^{-\beta}$ , we notice that the successor representation is equivalent to an unnormalized version of our transition estimates. Moreover, the same mathematical form crops up in complex network theory, where it is known as the communicability between nodes in a graph.<sup>19,67,68</sup>

The relationship between the transition estimates in our model and the successor representation is fascinating, especially given the marked differences in the concepts that the two models are based upon. In our model, people attempting to learn the one-step transition structure  $A$  instead arrive at the erroneous estimate  $\hat{A}$  due to natural errors in perception and recall. By contrast, given a desired time-scale  $\gamma$ , the successor representation defines the optimal prediction of node occupancies into the future.<sup>58,72</sup> Interestingly, the successor representation has been linked to grid cells

and abstract representations in the hippocampus,<sup>19,41</sup> decision making in reward-based tasks,<sup>42,73</sup> and the temporal difference and temporal context models of learning and memory.<sup>45,58,72</sup> Across all of these contexts, the successor representation implicitly assumes that humans make optimal predictions about the future; however, our results show that a similar mathematical form can instead represent a person who simply attempts to predict one step into the future, but misses the mark due to natural errors in cognition. This biologically-plausible hypothesis of erroneous predictions highlights the importance of thinking carefully about the impact of mental errors on human learning.<sup>47,55,56</sup>

## References

1. Hyman, R. Stimulus information as a determinant of reaction time. *J. Exp. Psychol.* **45**, 188 (1953).
2. Sternberg, S. Memory-scanning: Mental processes revealed by reaction-time experiments. *Am. Sci.* **57**, 421–457 (1969).
3. Johnson-Laird, P. N. Mental models in cognitive science. *Cogn. Sci.* **4**, 71–115 (1980).
4. Saffran, J. R., Aslin, R. N. & Newport, E. L. Statistical learning by 8-month-old infants. *Science* **274**, 1926–1928 (1996).
5. Bousfield, W. A. The occurrence of clustering in the recall of randomly arranged associates. *J. Gen. Psychol.* **49**, 229–240 (1953).
6. Fiser, J. & Aslin, R. N. Statistical learning of higher-order temporal structure from visual shape sequences. *J. Exp. Psychol.* **28**, 458 (2002).
7. Friederici, A. D. Neurophysiological markers of early language acquisition: from syllables to sentences. *Trends Cogn. Sci.* **9**, 481–488 (2005).
8. Gopnik, A. & Wellman, H. M. Reconstructing constructivism: Causal models, bayesian learning mechanisms, and the theory theory. *Psychol. Bull.* **138**, 1085 (2012).
9. Tompson, S. H., Kahn, A. E., Falk, E. B., Vettel, J. M. & Bassett, D. S. Individual differences in learning social and non-social network structures. *J. Exp. Psychol. Learn. Mem.Cogn.* (2018).

10. Reynolds, J. R., Zacks, J. M. & Braver, T. S. A computational model of event segmentation from perceptual prediction. *Cogn. Sci.* **31**, 613–643 (2007).
11. Meyniel, F. & Dehaene, S. Brain networks for confidence weighting and hierarchical inference during probabilistic learning. *Proc. Natl. Acad. Sci. U.S.A.* 201615773 (2017).
12. Bekinschtein, T. A. *et al.* Neural signature of the conscious processing of auditory regularities. *Proc. Natl. Acad. Sci. U.S.A.* **106**, 1672–1677 (2009).
13. Dehaene, S., Meyniel, F., Wacongne, C., Wang, L. & Pallier, C. The neural representation of sequences: from transition probabilities to algebraic patterns and linguistic trees. *Neuron* **88**, 2–19 (2015).
14. Piantadosi, S. T., Tenenbaum, J. B. & Goodman, N. D. Bootstrapping in a language of thought: A formal model of numerical concept learning. *Cognition* **123**, 199–217 (2012).
15. Tenenbaum, J. B., Griffiths, T. L. & Kemp, C. Theory-based bayesian models of inductive learning and reasoning. *Trends Cogn. Sci.* **10**, 309–318 (2006).
16. Newman, M. E. The structure and function of complex networks. *SIAM Rev.* **45**, 167–256 (2003).
17. Gómez, R. L. Variability and detection of invariant structure. *Psychol. Sci.* **13**, 431–436 (2002).
18. Newport, E. L. & Aslin, R. N. Learning at a distance I. statistical learning of non-adjacent dependencies. *Cogn. Psychol.* **48**, 127–162 (2004).



19. Garvert, M. M., Dolan, R. J. & Behrens, T. E. A map of abstract relational knowledge in the human hippocampal–entorhinal cortex. *Elife* **6** (2017).
20. Cleeremans, A. & McClelland, J. L. Learning the structure of event sequences. *J. Exp. Psychol. Gen.* **120**, 235 (1991).
21. Gomez, R. L. & Gerken, L. Artificial grammar learning by 1-year-olds leads to specific and abstract knowledge. *Cognition* **70**, 109–135 (1999).
22. Schapiro, A. C., Rogers, T. T., Cordova, N. I., Turk-Browne, N. B. & Botvinick, M. M. Neural representations of events arise from temporal community structure. *Nat. Neurosci.* **16**, 486–492 (2013).
23. Karuza, E. A., Thompson-Schill, S. L. & Bassett, D. S. Local patterns to global architectures: influences of network topology on human learning. *Trends Cogn. Sci.* **20**, 629–640 (2016).
24. Kahn, A. E., Karuza, E. A., Vettel, J. M. & Bassett, D. S. Network constraints on learnability of probabilistic motor sequences. *Nat. Hum. Behav.* **2**, 936 (2018).
25. Karuza, E. A., Kahn, A. E. & Bassett, D. S. Human sensitivity to community structure is robust to topological variation. *Complexity (In Revision)* (2019).
26. Tversky, A. & Kahneman, D. Judgment under uncertainty: Heuristics and biases. *Science* **185**, 1124–1131 (1974).
27. de Camp Wilson, T. & Nisbett, R. E. The accuracy of verbal reports about the effects of stimuli on evaluations and behavior. *Soc. Psychol.* 118–131 (1978).

28. Vinje, W. E. & Gallant, J. L. Sparse coding and decorrelation in primary visual cortex during natural vision. *Science* **287**, 1273–1276 (2000).
29. Tononi, G., Sporns, O. & Edelman, G. M. A measure for brain complexity: relating functional segregation and integration in the nervous system. *Proc. Natl. Acad. Sci. U.S.A.* **91**, 5033–5037 (1994).
30. Cohen, J. D., McClure, S. M. & Angela, J. Y. Should i stay or should i go? how the human brain manages the trade-off between exploitation and exploration. *Philos. Trans. R. Soc. Lond., B, Biol. Sci.* **362**, 933–942 (2007).
31. Wickelgren, W. A. Speed-accuracy tradeoff and information processing dynamics. *Acta Psychol.* **41**, 67–85 (1977).
32. Jaynes, E. T. Information theory and statistical mechanics. *Phys. Rev.* **106**, 620 (1957).
33. Friston, K., Kilner, J. & Harrison, L. A free energy principle for the brain. *J. Physiol. Paris* **100**, 70–87 (2006).
34. Ortega, P. A. & Braun, D. A. Thermodynamics as a theory of decision-making with information-processing costs. *Proc. R. Soc. A* **469**, 20120683 (2013).
35. Shannon, C. E. A mathematical theory of communication. *Bell Syst. Tech. J.* **27**, 379–423 (1948).
36. Brown, G. J. & Cooke, M. Computational auditory scene analysis. *Comput. Speech Lang.* **8**, 297–336 (1994).

37. Lake, B. M., Salakhutdinov, R. & Tenenbaum, J. B. Human-level concept learning through probabilistic program induction. *Science* **350**, 1332–1338 (2015).
38. McCarthy, G. & Donchin, E. A metric for thought: a comparison of p300 latency and reaction time. *Science* **211**, 77–80 (1981).
39. Karuza, E. A., Kahn, A. E., Thompson-Schill, S. L. & Bassett, D. S. Process reveals structure: How a network is traversed mediates expectations about its architecture. *Sci. Rep.* **7**, 12733 (2017).
40. Baayen, R. H., Davidson, D. J. & Bates, D. M. Mixed-effects modeling with crossed random effects for subjects and items. *J. Mem. Lang.* **59**, 390–412 (2008).
41. Stachenfeld, K. L., Botvinick, M. M. & Gershman, S. J. The hippocampus as a predictive map. *Nat. Neurosci.* **20**, 1643 (2017).
42. Momennejad, I. *et al.* The successor representation in human reinforcement learning. *Nat. Hum. Behav.* **1**, 680 (2017).
43. Boas, M. L. *Mathematical methods in the physical sciences* (Wiley, 2006).
44. Gregory, R. L. Perceptions as hypotheses. *Phil. Trans. R. Soc. Lond. B* **290**, 181–197 (1980).
45. Howard, M. W. & Kahana, M. J. A distributed representation of temporal context. *J. Math. Psychol.* **46**, 269–299 (2002).
46. Howard, M. W. & Kahana, M. J. Contextual variability and serial position effects in free recall. *J. Exp. Psychol. Learn. Mem. Cogn.* **25**, 923 (1999).

47. Richards, B. A. & Frankland, P. W. The persistence and transience of memory. *Neuron* **94**, 1071–1084 (2017).
48. Ortega, P. A. & Stocker, A. A. Human decision-making under limited time. In *Adv. Neural Inf. Process. Syst.*, 100–108 (2016).
49. Griffiths, T. L., Lieder, F. & Goodman, N. D. Rational use of cognitive resources: Levels of analysis between the computational and the algorithmic. *Top. Cogn. Sci.* **7**, 217–229 (2015).
50. Gershman, S. J., Horvitz, E. J. & Tenenbaum, J. B. Computational rationality: A converging paradigm for intelligence in brains, minds, and machines. *Science* **349**, 273–278 (2015).
51. Shenhav, A. *et al.* Toward a rational and mechanistic account of mental effort. *Annu. Rev. Neurosci.* **40**, 99–124 (2017).
52. Grimmett, G. & Stirzaker, D. *Probability and random processes* (Oxford university press, 2001).
53. Neter, J., Kutner, M. H., Nachtsheim, C. J. & Wasserman, W. *Applied linear statistical models*, vol. 4 (Irwin Chicago, 1996).
54. Seber, G. A. & Lee, A. J. *Linear regression analysis*, vol. 329 (John Wiley & Sons, 2012).
55. Collins, A. G. & Frank, M. J. How much of reinforcement learning is working memory, not reinforcement learning? A behavioral, computational, and neurogenetic analysis. *Eur. J. Neurosci.* **35**, 1024–1035 (2012).

56. Collins, A. G. & Frank, M. J. Within-and across-trial dynamics of human EEG reveal cooperative interplay between reinforcement learning and working memory. *Proc. Natl. Acad. Sci. U.S.A.* 201720963 (2018).
57. Dayan, P. Improving generalization for temporal difference learning: The successor representation. *Neural Comput.* **5**, 613–624 (1993).
58. Gershman, S. J., Moore, C. D., Todd, M. T., Norman, K. A. & Sederberg, P. B. The successor representation and temporal context. *Neural Comput.* **24**, 1553–1568 (2012).
59. Whitehead, S. D. & Lin, L.-J. Reinforcement learning of non-markov decision processes. *Artif. Intell.* **73**, 271–306 (1995).
60. Wang, X. & McCallum, A. Topics over time: a non-markov continuous-time model of topical trends. In *SIGKDD*, 424–433 (ACM, 2006).
61. Wolfe, J. M., Horowitz, T. S. & Kenner, N. M. Cognitive psychology: rare items often missed in visual searches. *Nature* **435**, 439 (2005).
62. Tria, F., Loreto, V., Servedio, V. D. P. & Strogatz, S. H. The dynamics of correlated novelties. *Sci. Rep.* **4**, 5890 (2014).
63. Baddeley, A. D. & Hitch, G. The recency effect: Implicit learning with explicit retrieval? *Mem. Cogn.* **21**, 146–155 (1993).
64. Arenas, A., Diaz-Guilera, A. & Pérez-Vicente, C. J. Synchronization reveals topological scales in complex networks. *Phys. Rev. Lett.* **96**, 114102 (2006).

65. Guimera, R., Danon, L., Diaz-Guilera, A., Giralt, F. & Arenas, A. Self-similar community structure in a network of human interactions. *Phys. Rev. E* **68**, 065103 (2003).
66. Ravasz, E. & Barabási, A.-L. Hierarchical organization in complex networks. *Phys.Rev. E* **67**, 026112 (2003).
67. Estrada, E. & Hatano, N. Communicability in complex networks. *Phys. Rev. E* **77**, 036111 (2008).
68. Estrada, E., Hatano, N. & Benzi, M. The physics of communicability in complex networks. *Phys. Rep.* **514**, 89–119 (2012).
69. Schall, R. Estimation in generalized linear models with random effects. *Biometrika* **78**, 719–727 (1991).
70. Hox, J. J., Moerbeek, M. & van de Schoot, R. *Multilevel analysis: Techniques and applications* (Routledge, 2017).
71. Bates, D., Mächler, M., Bolker, B., Walker, S. *et al.* Fitting linear mixed-effects models using lme4. *J. Stat. Softw.* **67** (2015).
72. Sutton, R. S. Td models: Modeling the world at a mixture of time scales. In *Machine Learning Proceedings 1995*, 531–539 (Elsevier, 1995).
73. Russek, E. M., Momennejad, I., Botvinick, M. M., Gershman, S. J. & Daw, N. D. Predictive representations can link model-based reinforcement learning to model-free mechanisms. *PLOS Comput. Biol.* **13**, e1005768 (2017).